

1 Geomorphological and morpho-sedimentary features of a sand  
2 barrier in a tectonically asymmetrical estuary during the Late  
3 Holocene: La Algaida (SW Spain)

4

5 Antonio Rodríguez-Ramírez <sup>a\*</sup>, José N. Pérez-Asensio <sup>b</sup>, Juan J.R. Villarías-  
6 Robles <sup>c</sup>

7

8

9 <sup>a</sup> Departamento de Ciencias de la Tierra, Facultad de Ciencias Experimentales, Campus de El Carmen,  
10 Universidad de Huelva, Avda. de las Fuerzas Armadas s/n, 21007 Huelva, Spain. arodri@uhu.es

11 <sup>b</sup> Departamento de Estratigrafía y Paleontología, Facultad de Ciencias, Universidad de Granada, Avda.  
12 Fuentenueva s/n, 18002 Granada, Spain

13 <sup>c</sup> Departamento de Antropología, Instituto de Lengua, Literatura y Antropología, Consejo Superior de  
14 Investigaciones Científicas (CSIC), Calle Albasanz 26-28, 28037 Madrid, Spain

15

16

17 [Pre-print version; please cite the printed typescript as:

18 “Geomorphological and morpho-sedimentary features of a sand barrier in a tectonically  
19 asymmetrical estuary during the Late Holocene: La Algaida (SW Spain),” by Antonio  
20 Rodríguez-Ramírez, José N. Pérez-Asensio, and Juan J. R. Villarías-Robles.

21 *Geomorphology* 432 (July, 2023) 108711.

22 <https://doi.org/10.1016/j.geomorph.2023.108711>

23

24

25

26

27

28

29 A B S T R A C T

30

31 Analysis of a number of drill cores, geomorphic patterns, and radiocarbon assays on  
32 mollusk shells from La Algaida spit, in the estuary of the Guadalquivir River (SW Spain),  
33 has revealed the genesis and evolution of a sandy barrier located in a rather complex neo-  
34 tectonic setting: the geological boundary between the Alpine belt of the Baetic mountain  
35 ranges and the Hercynian massif. The development of this sandy barrier during the Late  
36 Holocene has been conditioned by the presence, on the eastern bank of the estuary, of a  
37 Plio-Pleistocene paleo-relief which forms part of a raised block in a set of reverse-fault  
38 systems with SW-NE alignment, the most conspicuous of which is that of the Lower  
39 Guadalquivir Fault (LFG). These systems have influenced the morpho-stratigraphic and  
40 geomorphological disposition of the Holocene sediments on both sides of the tectonic  
41 alignment. The evidence presented here indicates that La Algaida spit is part of this raised  
42 tectonic block. As signs of subsidence are negligible, the spit exhibits series of exposed  
43 progradation units which started to develop shortly after the spit itself emerged, in the  
44 form of a barrier island. By contrast, subsidence processes affecting the Doñana spit, on  
45 the western bank of the estuary, are clearly marked, as they were sustained and massive.  
46 This asymmetry explains the relatively meager thickness, 22 to 24 m, of the sedimentary  
47 formations constituting La Algaida. Deposits at this location began to accumulate in about  
48 6000-5500 cal. BP, originally as part of extensive shoals lying on top of the Plio-  
49 Pleistocene paleo-relief. At present, the spit exhibits three exposed progradation units  
50 (PS). Punctuated by erosive discontinuities, these units, or phases, succeeded one another  
51 until the Roman period (PS1 and PS2); thereafter, a tombolo formed to connect the  
52 erstwhile barrier island with the mainland (PS3). The peculiar, tectonically conditioned,  
53 active asymmetry —geomorphological as well as sedimentary— in the Guadalquivir

54 estuary and its environs contradicts received geological understandings of the area, yet  
55 helps understand comparable transformations in other coastal areas of the planet.

56

57 *Keywords:*

58 Littoral geomorphology

59 Morpho-sedimentary infilling

60 Holocene

61 Guadalquivir estuary

62 South-west Spain

63

## 64 **1. Introduction**

65

66 The Holocene formations that shape the geography of present-day estuaries are  
67 extraordinary markers of the geodynamic processes that have been at work in coastal  
68 environments over the most recent thousands of years (Morales, 2022). Best known and  
69 most cited among these processes are those animated by rivers and the sea, which jointly  
70 impinge upon the geomorphological configuration of landscapes. Though less  
71 conspicuous in the literature, the processes derived from neo-tectonics affecting the same  
72 formations should not be neglected (Jackson, 2013), as such processes, including growth  
73 faults, have been shown to be significant contributors to subsidence and sedimentation  
74 (Dokka, 2011; Yeager et al., 2012). Neo-tectonics can be an important factor in the paleo-  
75 geography of an estuary, accounting for the extent to which it is filled in by sediments  
76 and explaining the location of depocenters, the markers of the local variations of sea level.  
77 It is important, too, in determining the geomorphological configuration that ensues in  
78 every phase of the process.

79

80 The Iberian side of the Gulf of Cádiz is punctuated by a number of estuaries. From west  
81 to east, the largest estuaries are those of the rivers Guadiana, Tinto-Odiel, Guadalquivir,  
82 Guadalete, and Barbate (Fig. 1). Of these five, the Guadalquivir estuary is by far the most  
83 extensive. In addition, it is distinct in that it lies in the area of transition between two very  
84 different geological domains: the Iberian massif and the Alpine belt of the Baetic  
85 mountain ranges, which is still active (González-Castillo et al., 2015). A rare case of  
86 morpho-structural asymmetry of this kind worldwide, the estuaries to the west of the  
87 Guadalquivir, pertaining to the rivers Tinto-Odiel and Guadiana, are part of the Iberian  
88 massif, whereas those lying further east, of the rivers Guadalete and Barbate, belong to  
89 the belt of the Baetic mountain ranges. Elsewhere on the planet, asymmetric domains of  
90 this kind are found on the Pacific coasts of America (Muhs et al., 1992; Ota and  
91 Yamaguchi, 2004) and in the Mediterranean basin (Vött, 2007; Mastronuzzi and Sansó,  
92 2012), where neo-tectonic processes wield a powerful control over the morpho-  
93 stratigraphy and geomorphological configuration of transitional areas of this nature.

94

95 The Holocene formations in the lower Guadalquivir River Basin, namely an extensive  
96 marshland and two littoral spits, Doñana and La Algaida, have been studied in detail in  
97 terms of its geomorphological evolution (Zazo et al., 1994; Rodríguez-Ramírez et al.,  
98 1996; Rodríguez-Ramírez and Yáñez, 2008; Rodríguez-Ramírez et al., 2015), the  
99 sedimentary infilling (Lario et al., 2001, 2002; Pozo et al., 2010), and neo-tectonics  
100 (Salvany et al., 2011; Rodríguez-Ramírez et al., 2014). This multi-faceted and extensive  
101 research has focused essentially on the formations lying on the western bank of the  
102 estuary, that is, on the littoral spit of Doñana and the marshland. By contrast, the littoral  
103 spit of La Algaida, on the eastern bank of the estuary, has been given far less attention.

104 Although this spit has been argued for as the most likely location of the political center  
105 of the pre-Roman realm of Tartessus (Barbadillo-Delgado, 1951; Villarías-Robles and  
106 Rodríguez-Ramírez, 2019), fieldwork has to date resulted in no more than a chronological  
107 outline of its geomorphological formations (Rodríguez-Ramírez et al., 1996, 2016). This  
108 study worked on the assumption that the position of the La Algaida spit is homologous to  
109 that of the Doñana spit, and that the morpho-sedimentary and geomorphological  
110 configurations of the former have thus been conditioned by the same morpho-structural  
111 parameters as those constraining the latter.

112

113 Given these circumstances in the literature, the specific objectives of our study were: 1)  
114 to determine the conditions that resulted in the genesis and location of La Algaida spit in  
115 the Guadalquivir estuary in the course of the Late Holocene; 2) to analyze the  
116 geomorphological and morpho-sedimentary evolution of this spit; 3) to describe and  
117 interpreting its facies distribution; 4) to characterize the influence of marine and estuarine  
118 conditions on the spit based on its paleontological content; and 5) to establish a robust  
119 chronology in order to understand the different phases of evolution of this formation. In  
120 carrying out the study, we conceived of La Algaida as a distinct research case from that  
121 of the more studied Doñana spit, located on the western side of the estuary and in a neo-  
122 tectonic context of subsidence. Nevertheless, the case of La Algaida can be used as a  
123 model for research into comparable estuaries in tectonically asymmetrical settings  
124 elsewhere in the world.

125

126

127

128

129 **2. Morpho-dynamic setting**

130

131 The Guadalquivir Estuary, at the midpoint of the Gulf of Cádiz, in the Atlantic Ocean,  
132 spreads out across an area of 1,800 km<sup>2</sup> (Fig. 1). Because of its geo-biodiversity and  
133 cultural history, it is an environment that elicits considerable interest. Some 700 km<sup>2</sup> of  
134 the area is protected under the name “Espacio Natural de Doñana,” which includes the  
135 renowned Doñana National Park, a UNESCO MAB Biosphere Reserve.

136

137 From a geomorphological standpoint, the Guadalquivir Estuary is flanked by the above-  
138 mentioned littoral spits, Doñana and La Algaída. The marshland behind them extends  
139 more than 80 km into the hinterland (Rodríguez-Ramírez et al., 2019). The Doñana spit,  
140 attached to the western bank of the estuary and oriented toward the SSE, is the largest  
141 coastal barrier in Spain; it is some 23 km long and 3.5 to 5.2 km wide, depending on the  
142 meridian. The Algaída spit, on the eastern bank of the estuary and oriented toward the  
143 NNE, is some 10 km long and 1.2 to 2.2 km wide. Both spits are largely covered by dune  
144 systems. Those spreading across the Doñana spit are particularly striking and active, to  
145 the extent that they only spare the most recent developments in the progradation of the  
146 spit in the form of successive littoral strands. The marshland behind the two spits features  
147 a number of levees and cheniers (Rodríguez-Ramírez and Yáñez, 2008), which are the  
148 byproduct of the intense fluvio-marine dynamics experienced by the estuary in the course  
149 of the Holocene. The sedimentary infilling of the estuary has been the work of the  
150 convergent rivers, chiefly the Guadalquivir advancing toward the ocean in the form of a  
151 large bird-foot delta in a low-energy environment.

152

153 At present, the hydrodynamic processes in the estuary are controlled by the fluvial regime,  
154 the tidal inflow, wave action, and drift currents. The Guadalquivir River is the axis of the  
155 largest fluvial network in SW Spain. The mean annual flow is 116.5 m<sup>3</sup>/s (Confederación  
156 Hidrográfica del Guadalquivir, 2016), in the wintertime ordinarily rising to 5,000 m<sup>3</sup>/s  
157 —extraordinarily as much as 10,000 m<sup>3</sup>/s— before the large transformations in the river  
158 basin during the 20<sup>th</sup> century (Vanney, 1970). The average tidal range at the outlet of the  
159 river is 2 m, with a maximum of 3.86 m (Spanish Ministry of Fomento, 2005). Average  
160 wave height, generated by southwesterly winds, is 0.6 m, although occasional storm  
161 surges in the Atlantic may unleash highly destructive erosive processes on the seashores  
162 (Rodríguez-Ramírez et al., 2003). In addition, waves raised in succession may be part of  
163 longshore drift currents that result in net transport of sediments from W to E. This  
164 movement of marine sediments turns NE on the shores of Sanlúcar de Barrameda, thus  
165 conditioning the progradation of La Algaida spit (Fig. 1).

166

### 167 **3. Tectonic setting**

168

169 One of the distinguishing traits of the Guadalquivir estuary is its location in the area where  
170 the European and the African plates converge, making it an area of high tectonic activity  
171 (González Castillo et al., 2015) (Fig. 1). Ever since the Miocene, the lower Guadalquivir  
172 River Basin has been subject to a rather notable tectonic conditioning (Salvany et al.,  
173 2011). This conditioning has generated a specific morpho-sedimentary disposition  
174 throughout the Quaternary (Flores-Hurtado, 1993; Rodríguez-Ramírez et al., 2014).  
175 Newly continuous GPS data (2008–2013), gathered at the Topo-Iberia stations in the  
176 western Baetic mountain ranges, reveal a rather consistent westward motion of these  
177 ranges with respect to the relatively stable Iberian Massif foreland (González Castillo et

178 al., 2015). These data have enabled researchers to recognize an area undergoing a  
179 contraction in the westernmost sector of the ranges. This contraction would have resulted  
180 in a deformation band affected mainly by folds, convergence toward the NW, and reverse  
181 faults that have been active at least since the Late Miocene. The most important of these  
182 faults is the Lower Guadalquivir River Fault (LGF) (Viguier, 1977; Armijo et al., 1977).  
183 Coupled with the mountain front of the Baetic ranges (Fig. 1B), this fault runs across the  
184 southernmost boundary of the Guadalquivir estuary. The line of convergence between the  
185 European and the African plates exhibits a dextral slip (Medialdea et al., 2009). In the  
186 Early–Middle Miocene, such a slip generated the radial arrangement of extensive  
187 allochthonous masses, known as “the Olistostrome Unit” (Torelli et al., 1997; Maldonado  
188 et al., 1999), in the Gulf of Cádiz, as well as in the Guadalquivir River Basin. The location  
189 of this formation on the Atlantic littoral of southern Iberia has been linked to the migration  
190 of the Alborán volcanic islet toward the west as a consequence of a formerly active  
191 subduction zone off the Mediterranean coast of Andalusia (Royden, 1993; Iribarren et al.,  
192 2007). Gutscher et al. proposed (2002) that this subduction is still active west of the Strait  
193 of Gibraltar.

194

195 North of the LGF, in the foreland of the Iberian Massif, where the Doñana spit and most  
196 of the marshland of the lower Guadalquivir River Basin extend, the area features a  
197 complex system of N-S oriented faults that are joined by subordinate E-W oriented faults  
198 (Viguier, 1977; Armijo et al., 1977). A set of additional, secondary alignments, oriented  
199 NW-SE and NE-SW, has been identified by other researchers (e.g., Flores-Hurtado, 1993;  
200 Salvany, 2004); these secondary alignments crisscross the northern block of the LGF-  
201 affected area. The same researchers also recognized a regional tilting of the basin toward  
202 the SSE, which bears strongly on the sedimentary and geomorphological pattern of the  
203 Holocene formations in the basin. The overall effect of this process of subsidence is the



204 accumulation of increasingly massive depocenters as one moves toward the southernmost  
205 sector of the estuary and its vicinity. South of the LGF, in the mountain frontal areas,  
206 where La Algaida spit lies, recent geological structures and seismicity have resulted in  
207 moderate deformation from compressional stress, aligned roughly NW–SE to WNW–  
208 ESE (González Castillo et al., 2015).

209

## 210 **4. Materials and methods**

211

### 212 *4.1. Geomorphology*

213

214 We analyzed aerial photographs, generated by photogrammetric flights over Spain in  
215 1956 and 1957 by U.S. planes, so as to reconstruct the general geomorphological features  
216 of the natural configuration of the lower Guadalquivir River Basin up to that date, before  
217 the large transformations in the area that took place over the following decades. We then  
218 analyzed in detail topographic data in a digital model from a Light Detection and Ranging  
219 (LIDAR) survey from 2018, in addition to the use of the program Global Mapper. Our  
220 aim was to gather precise geomorphological information on the different formations  
221 recognized in the 1956/7 photographs. We supplemented the analysis of these  
222 photographs and that of the 2018 LIDAR model with direct observations in the field.

223

### 224 *4.2. Lithostratigraphy*

225

226 In 2021, we drilled the spit deposit to obtain two cores, A1 and A2, for the purpose of  
227 accessing the sedimentary configuration and facies of the Holocene formations under  
228 study (Fig. 1). Core A1, to a depth of 27 m, was extracted at 36°51'42.85''N and

229 6°18'38.47''W, while core A2, to a depth of 29 m, was dug out at 36°52'27''N and  
230 6°17'28''W (Fig. 1). In addition, we analyzed two other cores, A3 and A4, from a  
231 previous construction project that required geotechnics. Core A3, to a depth of 10 m, had  
232 been obtained at 36°52'57.34''N and 6°16'56.79''W, while core A4, to a depth of 14 m,  
233 had been extracted at 36°49'51.05''N and 6°19'12.56''. All four boreholes were drilled  
234 by a direct circulation rotary method, with continuous core sampling.

235

236 We identified the sedimentary facies and then described the morphology, geometry, and  
237 relationships of these facies to one another. The elevations in the facies refer to the mean  
238 sea level (msl) in the Gulf of Cádiz. We performed grain-size analyses using conventional  
239 sieving for particle sizes >2 mm and utilized a Malvern Mastersizes 2000 laser diffraction  
240 particle analyzer for smaller fractions, from 2 mm down to 2 µm. We then applied  
241 Shepard's sediment classification to grain-size results (Shepard, 1954) in order to  
242 describe sediment texture, including sand, silt, and clay fractions.

243

#### 244 *4.3. Paleontology*

245

246 We used the general qualitative taxonomy applicable to malacofauna (Gofas et al., 2017)  
247 on sediment samples from the cores, 14 from A1 and 19 from A2. We washed the  
248 samples, around 12 cm<sup>3</sup> per sample, employing a 1 mm sieve. Although a large part of  
249 the remains thus retrieved turned out to be fragmented and worn out, we nevertheless  
250 sought to identify the malacofauna that were found to the species level as far as possible.  
251 Of note in the samples was also the relative abundance of other groups, including  
252 scaphopods, corals, and bryozoans.

253

254 We performed microfossil analyses on 21 sediment samples from A1 and 34 from A2.  
255 We weighed dried samples, wet-sieved them over a 63- $\mu\text{m}$  mesh, and dried them in an  
256 oven at 40°C. We then dry-sieved the samples over a mesh (>125- $\mu\text{m}$ ) in order to study  
257 planktic and benthic foraminifera.

258

259 We used the presence of specific planktic foraminiferal species, which are commonly  
260 used as bio-stratigraphic markers, in order to date Pliocene sediments. For benthic  
261 foraminiferal analyses, we obtained sub-samples containing at least 300 benthic  
262 foraminifera by using a micro-splitter. In addition, we differentiated Pliocene from  
263 Holocene benthic foraminifera on the basis of shell preservation and presence or absence  
264 of Pliocene planktic foraminiferal biomarkers. Poorer shell preservation (i.e., yellowish  
265 and frosty shells) and presence of Pliocene planktic biomarkers was indicative of Pliocene  
266 fauna, whereas Holocene fauna was characterized by better shell preservation (i.e., glassy  
267 shells) and the absence of Pliocene planktic foraminiferal species. We also differentiated  
268 Holocene marine from Holocene estuarine fauna by the ecology of each benthic  
269 foraminiferal species. Marine species included miliolids, keeled *Elphidium* spp.,  
270 *Ammonia beccarii*, *Asterigerinata* spp., *Cibicides* spp., *Cibicidoides* spp., *Rosalina* spp.,  
271 and other marine species (Murray, 1991, 2006; Mendes et al., 2004). Estuarine species  
272 included *Ammonia tepida*, *Haynesina germanica* and unkeeled *Elphidium* spp. (Murray,  
273 1991, 2006; Debenay, 1995, Blázquez and Usera, 2010; Pérez-Asensio and Aguirre,  
274 2010; Pérez-Asensio and Rodríguez-Ramírez, 2020). Finally, we calculated benthic  
275 foraminiferal abundance (N/g) by totaling the number of benthic foraminifera per gram  
276 of dry sediment. We computed the planktic/benthic ratio (P/B) as the score of  $[P/(P+B)]$   
277 x 100.

278

279 *4.4. Dating*

280

281 We obtained eight radiocarbon dates from mollusk shells at the Accium BioSciences  
282 Accelerator Mass Spectrometry Laboratory (Seattle, USA), in addition to the use of  
283 published radiocarbon data (Rodríguez-Ramírez et al., 1996) (Table 1). Shells were  
284 selected that showed minimal, or no, transportation, and which had been preserved as  
285 articulated valves in the sedimentary record. For calibration of the radiocarbon data, we  
286 relied on version 8.2 of the CALIB program (Stuiver & Reimer, 1993), in addition to the  
287 calibration dataset of Heaton et al. (2020). Uncertainties in the calibrated ages are  
288 expressed in Table 1 as  $2\sigma$  errors. We made corrections for the reservoir effect by using  
289 the  $\Delta R$  values recommended by Soares (2015). He suggests a  $\Delta R$  value of  $-108 \pm 31$  14C  
290 yr for the late Holocene on the Andalusian coast of the Gulf of Cádiz, except for the years  
291 4400–4000 14C yr BP, for which he recommends a  $\Delta R$  value of  $+100 \pm 100$  14C yr.

292

293 **5. Results**

294

295 *5.1. Geomorphology*

296

297 Analysis of the 2018 LIDAR images, along with the 1956/7 aerial photographs, enabled  
298 us to define in detail the geomorphological configuration of the research area (Fig. 2). We  
299 discovered that La Algaida spit is made up of morpho-sedimentary systems showing a  
300 three-phase succession of progradation. The oldest system identified (PS1), covered by  
301 an aeolian mantle of scant morphology, acted as a barrier island, to which the subsequent  
302 systems of progradation (PS2 and PS3) adhered.

303

304 These three systems of progradation turned out to be marked out from one another by  
305 erosive discontinuities that left geomorphological traces in the development of the littoral  
306 strands. The strands of the PS1 system prograded successively toward the NE,  
307 surrounding the central area of the barrier island and causing this island to grow toward  
308 the S. The most recent system (PS3) made it possible for the island to connect with the  
309 mainland in the last phases of progradation by means of a tombolo, thereby transforming  
310 the island into a spit. The littoral strands of PS2 and PS3 exhibit a series of dunes, with a  
311 foredune morphology, that relate to the erstwhile shorelines. Toward the hinterland of the  
312 spit, these dunes evolve into parabolic dunes, reaching a maximum elevation of some 15  
313 m. At present, the spit is surrounded by marshland on three sides away from the ocean;  
314 dynamically speaking, it is a relict formation.

315

## 316 *5.2. Lithostratigraphy and paleontology in the cores*

317

### 318 *5.2.1. Pre-Holocene deposits*

319

320 Below -15.5 m in core A1 and -18 m in core A2, we found sands, sandy silts, and yellow  
321 clayey silts (Fig. 3). These same facies were found below -8 m in core A4 and below -6  
322 m in core A3. In core A1, we retrieved sandy silts consisting of 15-25% sand, 55-65%  
323 silts, and 15-18% clay, and ochre in color (10YR6/8). Interspersed in the silts were thin  
324 deposits of more sand, lithified by carbonate. At the top, were carbonated nodules, very  
325 dusty and edaphic in nature. There were abundant remains of malacofauna, mainly of  
326 Ostreidae and Pectinidae, rather reworked. At the point of contact with the overlying gray  
327 sands in the core, there was a concentrated layer of pebbles of various kinds (including  
328 carbonate and quartzite), some of which were large (10 x 5 cm), and showed clear signs

329 of reworking and transportation. These facies included the planktic foraminiferal species  
330 *Globoconella puncticulata* and *Globorotalia margaritae*, suggesting an early Pliocene  
331 age between 4.52 and 3.81 Ma (Lourens et al., 2004; Pérez-Asensio et al., 2018). Also  
332 present in these facies, were poorly preserved benthic foraminiferal species, such as  
333 *Nonion faba* and *Ammonia beccarii*, typical of early Pliocene inner-middle shelf  
334 environments from the lower Guadalquivir River Basin (Murray, 1991, 2006; Pérez-  
335 Asensio et al., 2012). The relatively high P/B ratio values (~40% on average) (Fig. 3) are  
336 consistent with a fully marine early Pliocene inner-middle shelf setting.

337

338 In core A2, the clayey silts consisted of 5-10% sand, 70-75% silts, and 18-20% clay, and  
339 were ochre brown in color (7.5YR7/8). These silts reached a depth of -21,8 m, below  
340 which we found ochre (10YR6/8) sands (2-10% gravel, 45-70% sand, 10-35% silts, 10-  
341 15% clay), with lithified layers by carbonate in them. We identified no malacofauna in  
342 these sands, suggesting they may have been the product of a fluvial overflow.

343

344 The ochre clayey silts contained from 40 to 75% Pliocene faunal remains, consisting of  
345 early Pliocene planktic foraminiferal biomarkers (*G. puncticulata*, *G. margaritae*) and  
346 inner-middle shelf benthic foraminifera (*Nonion faba*, *Ammonia beccarii*) (Murray, 1991,  
347 2006; Lourens et al., 2004; Pérez-Asensio et al., 2012, 2018). This finding, along with  
348 that of a very low occurrence of benthic foraminiferal (N/g) (Fig. 3), suggests that the  
349 sample was made up of reworked Pliocene fauna that had been transported to the core  
350 site by fluvial dynamics. The source of this transported early Pliocene fauna could be the  
351 sands farther down the core, which showed higher percentages of Pliocene fauna and  
352 higher N/g. The lower stratigraphic position of the ochre clayey silts below the Holocene

353 facies indicates that these silts were deposited during the Pleistocene and that early  
354 Pliocene foraminifera were transported to the site in the process.

355

### 356 5.2.2. *Gray sands facies*

357

358 We encountered gray sand facies between approximately -9 m and -15.5 m in core A1,  
359 between -12 m and -18 m in core A2, and between -4 m and -8 m in core A4 (Fig. 3). In  
360 these facies, coarser layers alternated with finer ones. The coarser layers were  
361 characterized by their gray color (10YR7/1) and medium sands (5-10% gravel, 40-50%  
362 sand, 30-40% silts, 5–8% clay) that included carbonated dispersed pebbles of small size  
363 (maximum 2 x 1 cm) with quartzite. The finer, interspersed layers consisted of sandy silts  
364 of varying thickness, from 1 to 10 cm, and darker gray in color (10YR5/1). The silt  
365 component was appreciably larger: 3-5% gravel, 20-35% sand, 35-55% silts, 5–8% clay.

366

367 Dispersed within them we found remains of malacofauna, some showing clear signs of  
368 much reworking, while others were in good condition and far less reworked, especially  
369 in the darker gray-colored silty clays. We were able to recognize a number of various  
370 species, including *Ostrea* sp., *Corbula gibba*, *Cerastoderma* sp., *Chlamys* sp., *Tellina* sp.,  
371 *Nassarius* sp., *Clathroscala cancellata*, *Turbonilla* sp., *Murex* sp., and *Turritela* sp.,  
372 among fragments of corals and colonies of bryozoans.

373

374 In core A1, the foraminiferal data show an average P/B ratio of 7%, with an N/g of 35,  
375 and a composition of 74% marine fauna to 24% estuarine fauna (Fig. 3). Core A2 yielded  
376 an average P/B ratio of 18%, an N/g of 96, and a composition of 53% marine fauna and  
377 43% estuarine fauna (Fig. 3). In both cores, coarser layers produced more marine fauna

378 and lower N/g, whereas finer layers contained more estuarine fauna and higher N/g (Fig.  
379 3).

380

381 Judging by the dates obtained for the samples from cores A1 and A2, these gray sand  
382 facies would date from c. 5500 to c. 3600 cal BP (Table 1). These facies are the first  
383 formations of the Quaternary to rest directly on the Plio-Pleistocene paleo-relief.

384

### 385 5.2.3. *Yellow sands facies*

386

387 The base of the yellow sands facies was found at -9 m in core A1, -12 m in core A2, and  
388 2 m in core A4 (Fig. 3). They consisted of layers of coarse sands with abundant gravel  
389 that include interspersed packages of silty sands. The coarsest layers were comprised of  
390 rough, ochre yellowish-colored (10YR8/6) sands (20-30% gravel, 50-60% sand, 5-10%  
391 silts, 2-3% clay), with pebbles of various kinds, carbonated and quartzite, some of them  
392 as large as 6 x 8 cm in size. While in core A1 we discovered a larger concentration of  
393 gravel at a depth of -2 to -5 m, in core A2 we found a comparable concentration at a depth  
394 of -1 to -8 m. The interspersed layers of siltier sands had, in most cases, decimeter  
395 thicknesses, were light yellow in color (10YR8/3), and contained a rather high amount of  
396 silt, the total composition being 5-10% gravel, 30-40% sand, 35-45% silts, and 2-3% clay.

397

398 There were abundant remains of malacofauna, showing clear evidence of transportation  
399 and wear, as though they were no more than sedimentary debris. We were able to identify  
400 a number of species, most readily those with robust shells, better equipped to sustain  
401 wear. However, in the siltier layers we found remains that, though of smaller species,  
402 were better preserved. The species identified include *Glycimeris* sp., *Pecten* sp., *Chlamys*



403 sp., *Petricola* sp., *Tellina* sp., *Corbula* sp., *Chamelea* sp., *Cerithium* sp., *Nassarius* sp.,  
404 *Murex* sp., *Turritella* sp., *Clathroscala cancellata*, and scaphopods.

405

406 Foraminiferal data showed similar average values for marine (~70%) and estuarine  
407 (~30%) fauna in both cores, although the P/B ratio and N/g were lower in core A2 (Fig.  
408 3). In both cores, the coarser and finer layers showed similar values for marine (~70-75%)  
409 and estuarine (~25-30%) fauna, as well as similar P/B ratios (~3-6%) (Fig. 3). However,  
410 the N/g was higher in the finer layers in both cores (Fig. 3).

411

412 These yellow sand facies would date from c. 3600-3000 cal BP in core A2 and from c.  
413 3600-1700 cal BP in core A1 (Table 1). In core A4, these facies were generated by the  
414 most recent progradation.

415

#### 416 5.2.4. *Aeolian yellow sand facies*

417

418 We discerned an initial *Aeolian yellow sand* segment, which extended to a depth of -1.5  
419 m in cores A1 and A2, and to a depth of just -0.5 m in core A4. In this top segment, the  
420 facies were light yellow in color (10YR8/4) medium sands (78-82% sand, 10-15% silts,  
421 2-5% clay), very well sorted and containing no fossils. In core A2, these sands  
422 transitioned to deeper layers through a 15 cm-thick layer of dark brown (5YR4/6) silty  
423 sands of an edaphic nature, which contained organic matter in abundance.

424

#### 425 5.2.5. *Clayey facies*

426

427 In core A4, we found clayey facies from an elevation of +2 m down to a depth of -4 m,  
428 while in core A3, they ranged from the surface down to -6 m (Fig. 3). They were gray-  
429 greenish (10YR6/1) clayey silts (40–55% silt, 25–35% clay, 1–5% sand) with some rather  
430 meager, sandier deposits interspersed throughout. In core A4, these clayey silts appeared  
431 to separate the fine yellow sands from the gray sands. The malacofauna included mostly  
432 *Cerastoderma* sp., *Ostrea* sp., and *Tellina* sp., the latter in the sandier deposits. In core  
433 A3, these clayey sands rested directly on the Pliocene substructure, the malacofauna  
434 consisting mostly of *Cerastoderma* sp. and *Scobrucoloaria plana*, with concentrations of  
435 remains particularly abundant from -1 to -2 m.

436

## 437 **6. Discussion**

438

### 439 *6.1. Pre-Holocene formations (>11.7 ka) and tectonics*

440

441 The paleogeography of the research area has been strongly conditioned by the geological  
442 structures of the lower Guadalquivir River Basin (Fig. 1B and 4), where the Alpine belt  
443 of the Baetic mountain ranges meets the Hercynian massif of the Iberian Peninsula, and  
444 where the NW front of the Baetic ranges is still active. This front includes a deformation  
445 band affected by reverse faults (González-Castillo et al., 2015), such as the lower  
446 Guadalquivir River Fault (LGF) (Fig. 1B and 4). Such reverse faults mark the boundary  
447 between two very different domains: a raised block, south of the faults, and a sunken  
448 block, north of the faults.

449

450 Researchers have long assumed that the La Algaida spit, like the Doñana spit, formed part  
451 of the sunken block, north of the LGF (Rodríguez-Ramírez et al., 2014). However, the

452 cores extracting sedimentation from La Algaida spit and its milieu, described above,  
453 showed a shallow Pre-Holocene substratum from the Plio-Pleistocene at depths below  
454 msl in the Gulf of Cádiz of -16 in A1, -18 in A2, -6 m in A3, and -8 m in A4, all of which  
455 pertain to the raised block (Fig. 4). None of these formations is nowadays visible above  
456 sea level in the immediate vicinity of the spit.

457

458 Generally speaking, these formations define a platform-like paleo-relief which rests upon  
459 Miocene formations located farther south and spreads out under the spit. As one moves  
460 toward the N or W—that is, toward the sunken block north of the LGF—this paleo-relief  
461 rapidly loses elevation. This is consistent with the findings from other cores drilled in  
462 terrains where deposits from the Holocene are remarkably large (Rodríguez-Ramírez et  
463 al., 2014) (Fig. 4). The analysis of three cores from points off the north and west of La  
464 Algaida spit, described in Salvany et al. (2011), revealed the presence of the Plio-  
465 Pleistocene formations at great depths, below massive deposits from the Late Pleistocene  
466 and the Holocene (Fig. 4C). Such a significant contrast in depth between the two series  
467 of cores, on and off the spit, dramatically highlights the prominence of the paleo-relief  
468 that lies under the spit. Underneath the spit, the paleo-relief is found at comparatively  
469 rather shallow depths.

470

471 A system of faults and alignments oriented NNE-SSW (IGME, 1988), shapes the  
472 orographic configuration of the eastern side of the Guadalquivir estuary, which includes  
473 prominent hills and valleys. The hills can be as high as 70 m, while the valleys were  
474 flooded by the ocean until a few centuries ago (Rodríguez-Ramírez et al., 2015), when  
475 they became the marshes that characterize the area today. The Pliocene paleo-relief that  
476 extends underneath would have been subject to the same system of alignments. In effect,

477 both the LFG, along with other reverse faults with a similar SW-NE orientation  
478 (González-Castillo et al., 2015), and the array of NNE-SSW faults would have favored  
479 the formation of such a paleo-relief. The NNE-SSW faults would have moved slightly  
480 toward the north of the LGF, at the same time causing their own transit toward the sunken  
481 block, where the depocenter of the Holocene formations lies (Fig. 1B and 4A). This  
482 dynamic, in turn, would explain the odd meander that the Guadalquivir River traces near  
483 its mouth, turning northwards on a short detour, and thereafter head sharply south.

484

485 During periods of low sea level, such as the MIS2 Last Glacial Maximum (Dabrio et al.,  
486 2000), the subterranean paleo-relief would have stood high above sea level, like a hillock  
487 overlooking the eastern side of the Guadalquivir paleo-valley, subject to the regular action  
488 of the sea waves and the occasional flooding of transgressive events.

489

#### 490 *6.2. From shoal to barrier island (6000-5500 to 3600 cal BP)*

491

492 Unlike the formations to the north of the LGF, in which Holocene sedimentation is  
493 remarkably thick (Salvany et al., 2011; Rodríguez-Ramírez et al., 2014), the eastern side  
494 of the Guadalquivir estuary, south of the fault, where La Algaida spit is located, contains  
495 relatively thin Holocene deposits, amounting to as little as 22 m in core A1 and 24 m in  
496 core A2 (Fig. 4). The difference between the two locations, north and south of the LGF,  
497 highlights the sedimentary asymmetry affecting the coastal formations of the Late  
498 Holocene in the area. Whether marshes or sandy barriers, their morphology and  
499 magnitude clearly depend on which side of the LGF these formations lie on (Fig. 4).

500

501 As the sea level rose over the course of the MIS1 transgression, the Guadalquivir River  
502 Valley became increasingly flooded by the ocean, while the Plio-Pleistocene relief was  
503 gradually submerged and thereby became subject to the intense erosion generated by the  
504 marine dynamic. Characterized by low bathymetry and located at the outlet of the river,  
505 this relief would have served as threshold and trap for the sedimentary package of the  
506 maritime transgression as this package moved progressively toward the east during the  
507 sustained sea-level rise. Both the incessant erosive retreat of the coastline and the high  
508 availability of sediments favored this process.

509

510 The earliest facies from the Holocene deposited on top of such a structural high ground  
511 from the Plio-Pleistocene are rather coarse. They include a bed of pebbles of a diverse  
512 nature dragged from surfacing formations in the vicinity, as if constituting a marine  
513 transgressive lag. At the present-day mouth and its coastal environs, there are  
514 considerable littoral outcrops of calcarenites from the Plio-Pleistocene, many of which  
515 exhibit the morphology of shore platform (Fig. 1), and which, over thousands of years,  
516 fed large amounts of coarse sediments to the Holocene formations. Judging by  
517 radiometric assays on samples collected from the earliest of these formations resting on  
518 the Plio-Pleistocene paleo-relief, this process would have initiated in the time span from  
519 6000 to 5500 cal BP (Table 1) (Fig. 5a), or possibly some time earlier, during the phases  
520 that preceded the transgressive maximum established for the Gulf of Cádiz (Zazo et al.,  
521 2008; Rodríguez-Ramírez et al., 2015). Oceanic flooding of the paleo-relief would have  
522 taken place at the same time.

523

524 Following the coarse bed, various facies of gray sands and silts came to rest on the paleo-  
525 relief, accumulating over a period from about 5500 cal BP to about 3600 cal BP (Table

526 1). The malacofauna and foraminifera identified in the cores suggest a semiconfined,  
527 subtidal-intertidal milieu for the period, strongly indicative of an extensive shoal subject  
528 to river inputs while protected from the marine dynamics by means of a system of swash  
529 bars, the setting being an ebb tidal delta under strong influence of the swell (Fig. 5a, 6Aa  
530 and 6Ba). Within this semiconfined environment, the foraminiferal data show that less  
531 sheltered areas (core A1 site) (Fig. 3) had higher energy and received higher inputs of  
532 marine sediment than more sheltered areas (core A2 site). This is indicated by evidence  
533 including: (1) a lower P/B ratio, suggesting that less-resistant, delicate planktic  
534 foraminiferal shells were preferentially destroyed (Kucera, 2007; Pérez-Asensio et al.,  
535 2017; Pérez-Asensio, 2021); (2) lower N/g (i. e., more sediment supply); and (3) more  
536 abundant marine fauna in core A1 than in core A2 (Fig. 3).

537

538 While the siltiest deposits are indicative of phases of less energy affecting the  
539 environment, the sandiest, coarsest deposits would have been the work of events of higher  
540 energy, such as storm surges in wintertime, nowadays a frequent event in the Gulf of  
541 Cádiz (Rodríguez-Ramírez et al., 2003). This interpretation is supported by a higher  
542 number of marine benthic foraminiferal fauna and a lower N/g in the coarser layers,  
543 alongside a conversely higher number of estuarine benthic foraminiferal fauna and a  
544 higher N/g (Fig. 3) in the thinner layers. Dabrio et al. (2000), Lario et al. (2002), and  
545 Boski et al. (2008) independently argue that the time span 5500-3600 cal BP was also the  
546 primary phase of sedimentary accretion in the estuaries across the Gulf of Cádiz, when  
547 the most notable systems of littoral spits formed and started to prograde.

548

549 The yellow sand facies that followed this period are consistent with a foreshore-backshore  
550 environment that was more exposed to the open sea, as indicated by the high abundance

551 of marine benthic foraminifera (~70%) found in cores A1 and A2. Such facies would have  
552 been the product of a system of swash bars marking out the sea front of the ebb tidal delta,  
553 and thus subject to rather intense swell dynamics (Fig. 5a, 5b, 6Ba and 6Bb). Impelled by  
554 the longshore drift current, these swash bars would have migrated progressively toward  
555 the inner side of the estuary, where they would stabilize as extensive shoals and eventually  
556 surface to become littoral strands. The outcome of such a development, that is the  
557 formation of La Algaida as a barrier island, would date to the year 3600 cal BP or  
558 thereabouts (Table 1) (Fig. 5b). Progradation of this barrier island toward the ocean would  
559 explain the lower N/g and P/B ratios recorded in the more proximal core A2 (Fig. 3),  
560 suggesting higher sediment supply at this site. Sedimentological and geomorphological  
561 research into the estuary (Rodríguez-Ramírez et al., 1996; Lario et al., 2002; Rodríguez-  
562 Ramírez et al., 2015; Pérez-Asensio and Rodríguez-Ramírez, 2020) has revealed a  
563 transition to a more confined estuary in the years from c. 3400 to c. 3000 cal BP, when  
564 abundant sedimentation occurred far inland from the ocean by marine processes (Lario et  
565 al., 2001; Rodríguez-Ramírez et al., 2014, 2015, 2016).

566

567 As a barrier island in the Guadalquivir estuary, La Algaida was separated from the  
568 mainland by two ocean inlets (Menanteau, 1979, Rodríguez-Ramírez et al., 1996), which  
569 were also outlets of the Guadalquivir River: a very broad inlet, between the barrier island  
570 and the Doñana spit to the west, and a narrower inlet between the island and the Miocene  
571 reliefs to the south (Fig. 5b). These inlets left evidence of their presence in both the  
572 succeeding littoral strands surrounding La Algaida and the Doñana spit (Rodríguez-  
573 Ramírez et al., 2016). The flood-and-ebb tidal delta thus became split into two sectors  
574 according to the two inlets, with each sector separated from the other by the barrier island.  
575 This kind of dynamic system, comprising channels, shoals, and swash bars, has also been

576 recognized in other estuaries in the Gulf of Cádiz at the earliest stages of the Holocene  
577 evolution (Morales et al., 2006).

578

579 The sedimentation revealed by cores A1 and A2 indicates that such primeval sedimentary  
580 developments in La Algaida, following the transgressive maximum, pertain to what we  
581 refer to as “Prograding Unit 1 (PS1)” (Fig. 2), the oldest constituent of the barrier island  
582 (Fig. 2, 5, and 6). The first sediments making up PS1 accumulated in the form of slightly  
583 sloping depositional surfaces oriented toward the E-NE. This orientation resulted from  
584 both the previous paleo-topography from the Pliocene, some 3 m deeper in core A2 than  
585 in core A1, and the powerful migration of the sedimentary systems in the same direction  
586 (Fig. 4B). Due to these conditions, the earliest deposits in the Holocene at the La Algaida  
587 site yield older dates in core A1 than in core A2.

588

589 The emerging island, at present the most stable sector in the spit as well as the best  
590 protected from wintertime storm surges, features the archaeological site of El Tesorillo,  
591 which includes evidence of occupation from both the post-Tartessian, or Turdetanian,  
592 period in the 5th to 2nd centuries BCE, and the Roman imperial period from the mid-1st  
593 century BCE to the 4th century CE (Esteve-Guerrero, 1952; Blanco-Freijeiro and Corzo-  
594 Sánchez, 1983; López-Amador and Ruiz-Gil, 2010) (Fig. 2).

595

596 In the course of these formative developments, La Algaida was set in an estuary that was  
597 clearly dominated by a swell conditioned by intense drift currents along the coast,  
598 following a SW-NE direction on its eastern side and a NW-SE direction on its western  
599 side (Fig. 5). In the course of the Holocene, the disposition of these currents has facilitated  
600 incessant sedimentation toward the inner side of the estuary. Convergence of these



601 currents at the site of the structural high ground from the Plio-Pleistocene, where La  
602 Algaida formed, resulted in the emergence of the two-sector, swell-dominated flood-and-  
603 ebb tidal delta noted above, and the development of significant sandy barriers. This kind  
604 of complex process, affecting swell-dominated estuarine systems (Roy et al., 1980), has  
605 been recognized in other estuaries along the Gulf of Cádiz, including those of the rivers  
606 Guadalete and Guadiana (Morales et al., 2001, 2006), as well as other estuaries around  
607 the world (Dalrymple et al., 1992).

608

### 609 *6.3. From barrier island to spit (3600 to 1700 cal BP)*

610 Following the stabilization of the barrier island c. 3600 cal BP, from c. 3000 cal BP  
611 onwards the subsequent progradation units, PS2 and PS3, developed in the same swell-  
612 dominated estuarine system (Fig 5). These prograding littoral systems fed on the  
613 evolution of the swash bars in the two ebb tidal deltas that had formed in the two river  
614 outlets. Almost the entire uppermost record of the yellow sand facies in core A1 dates  
615 from this period, specifically from c. 3000 cal BP to c. 1650 cal BP (Table 1). In other  
616 estuaries on the Gulf of Cádiz this kind of development pertains to a phase of greater  
617 confinement, which has been determined to have begun after c. 3400-3000 cal BP (Zazo  
618 et al., 1994; Rodríguez-Ramírez et al., 1996; Lario et al., 2002; Rodríguez-Ramírez et al.,  
619 2015; Camacho et al., 2016; Pérez-Asensio and Rodríguez-Ramírez, 2020).

620

621 Prograding Unit PS2 developed as a build-up on PS1; a series of erosive scarps marks the  
622 geomorphological and sedimentary discontinuity between the two units (Fig. 2 and 5).  
623 The same geomorphological evidence makes it clear that Unit PS2 advanced mostly  
624 toward the NW and the SE from an older sedimentary structure. PS2 progradation resulted  
625 in a large geomorphological expansion over the length of the barrier island. Further

626 evidence of this process is provided by the successive littoral strands that mark out the  
627 spit on its westernmost side. Many of the formations that this process generated find  
628 themselves disjoined from one another by erosive scarps caused by the lateral migration  
629 of the fluvio-tidal channels in which the migration erosively incised La Algaida  
630 (Rodríguez-Ramírez et al., 2016). In turn, as in other estuaries along the Gulf of Cádiz  
631 (Morales et al., 2006), the intense wave dynamics caused the migration of the swash bars  
632 in the ebb tidal delta toward the backshore (Fig 5 and 6). By pushing the main fluvio-tidal  
633 channels toward the barrier inland, the continuous migration of the swash bars ended up  
634 eroding the boundaries of the island until they finally collapsed, allowing for the  
635 progradation of the system. More distal secondary channels then became functional and  
636 the process started anew.

637

638 The most recent evidence of the development of Unit PS2 seems to be the littoral strands  
639 of Los Prados, in the southeast (Fig. 2). These strands are the product of activity in the  
640 fluvio-tidal inlet channel east of the barrier island. It seems that this activity lasted until  
641 around 2050-1750 cal BP (Rodríguez-Ramírez et al., 2016), that is, until the first centuries  
642 of the Common Era. Writing in the late first century BCE about the uncertainty regarding  
643 the location of the pre-Roman city of Tartessus, Greek geographer-historian Strabo of  
644 Amasya (Str. 3.2.11; 1966) pointed out that the river *Baetis*, later Guadalquivir River, had  
645 two outlets or mouths, which suggests that the eastern tidal inlet of the ocean was still  
646 active at that time. Some fifty years later, geographer Pomponius Mela, a native of  
647 southern Iberia, apparently corroborated Strabo's testimony, writing (3.1.5; 1987) that the  
648 river *Baetis* reached the Atlantic Ocean by means of two large channels flowing from a  
649 large lake located not far from the sea, each of the channels being as large as the river  
650 itself before flowing into the lake.

651

652 Thereafter, a sand bar, or tombolo, formed south of the barrier island, a development of  
653 progradation phase PS3, resulting in the connection of the island with the mainland (Fig.  
654 5d and 6Ab). Prograding Unit PS3 turned out be the most extensive in La Algaida, and  
655 more generally in the Gulf of Cádiz (Dabrio et al., 2000; Lario et al., 2002; Camacho et  
656 al, 2016).

657

658 Over the past two millennia, progradation of the sandy barrier on the western bank of the  
659 estuary has been remarkable (Rodríguez-Ramírez et al., 1996, 2016), causing the Doñana  
660 spit to grow nearly 10 km in length and 4 km in width (Fig. 2 and 5). This process has  
661 been favored over these past two millennia by less intense subsidence of the Doñana spit  
662 (Rodríguez-Ramírez et al., 2014), while at the same time it has hindered the progradation  
663 of La Algaida.

664

665 During this last phase in the evolution of the Guadalquivir estuary, the littoral strands on  
666 the Doñana spit register a clearly marked erosive discontinuity in connection with a  
667 tsunami in the second or the third century CE (Rodríguez-Ramírez et al., 2016). La  
668 Algaida, however, has thus far failed to yield any evidence of this event, possibly due to  
669 the intensity of agriculture practices on the spit over the past two thousand years, which  
670 may have disfigured geomorphological patterns. In any event, attempting to correlate  
671 secondary patterns of progradation between the two spits seems an impossible task: La  
672 Algaida is subject to intense fluvio-tidal dynamics on the inner side of the Guadalquivir  
673 estuary, whereas Doñana is conditioned by the dynamic processes at work in the open  
674 sea.

675

676 In core A4 (Fig. 3), the transition of the facies from gray sands to estuarine clays  
677 substantiates the posited twofold process of ever greater confinement in the area of the  
678 paleo-estuary and subsequent closure of the eastern outlet of the Guadalquivir River. The  
679 facies of yellowish sands overlying the clays reveal both the migration of the tombolo  
680 eastward, energized by the swell, and the gradual collapse of the ebb tidal delta at this  
681 location (Fig. 5e, 6Ad, and 6Ae).

682

683 Thereafter, progradation continued on the western side of the spit only. The progressive  
684 displacement of the western channel of the estuary toward the NW facilitated this  
685 development (Fig. 5e). The considerable growth of the Doñana spit since the beginning  
686 of the Common Era, coetaneous with the PS3 phase in La Algaida spit, increasingly  
687 isolated the latter from the dynamic processes at work in the ocean (Rodríguez-Ramírez  
688 et al., 2016) (Fig 5). The end product of this development was the final disconnection of  
689 La Algaida from such processes and its resultant location in the shallow, more restrained  
690 water dynamics of the inner side of the estuary, a circumstance which selected  
691 sedimentation for clays as opposed to sands. At present, La Algaida is a relict component  
692 in the geomorphological dynamics of the Guadalquivir estuary and its environs (Fig. 2  
693 and 5f).

694

695 As sedimentation accrued to La Algaida in the course of the three phases of progradation  
696 that it experienced during the Late Holocene, the substratum from the Plio-Pleistocene  
697 underwent a slight isostatic subsidence. The offset in the largest depocenter ranges from  
698 8 to 10 m, as sedimentation in cores A1 and A2 reveals when compared with  
699 sedimentation in cores A4 and A3 (Fig. 1D).

700

701 6.4. The “island of Cartare” in the First Millennium BCE

702

703 The two outlets or mouths of the Guadalquivir River mentioned by the geographer-  
704 historian Strabo in the late first century BCE circumscribed an island which Strabo’s  
705 sources (chiefly Posidonius of Apamea and Artemidorus Ephesius) (García y Bellido,  
706 1993) believed had been the location of the city of Tartessus (Str. 3.2.11; 1966). The  
707 sedimentary, geophysical, and geomorphological evidence discussed above would appear  
708 to indicate that this island was La Algaida in the PS2 phase of progradation (Fig. 5c).  
709 Posidonius of Apamea and Artemidorus Ephesius spent some time in the area early in the  
710 first century BCE (García y Bellido, 1993). In his poem *Ora Maritima* (205-295; Avienus  
711 in Gavala y Laborde, 1959), the fourth-century CE Roman author Rufus F. Avienus  
712 conveyed an old tradition, likely from as early as the sixth century BCE, that this island  
713 was called “Cartare,” a place-name of Phoenician etymology which means “the island of  
714 the city”. Elements of this tradition included at least a portolan chart, or rutter, from a  
715 long-distance seafarer, probably Greek (Peretti, 1979; Villalba i Varneda, 1986;  
716 Domínguez Monedero, 1996, 2013; Villariás-Robles and Rodríguez-Ramírez, 2019).  
717 Indeed, the rutter-like narrative taken by much of Avienus’ poem suggests that the island,  
718 visible from the sea, stood close to the outlets of the river. The river surrounded the island  
719 after flowing from the hinterland into a lake called “*Lacus Ligustinus*.” The geography of  
720 the outlets and their vicinity was complex; the poem reads that, east of the island, the river  
721 distributed part of its flow into the nearby lands by means of three inlets. South of the  
722 island, after an apparently sequential bifurcation within a delta (“*ore bis gemino*,”  
723 “through a twice two-fold outlet”), the eastern channel rejoined the western channel and  
724 then flowed into the ocean.

725

726 The complexity of “a twice two-fold outlet” to the south of the island mentioned in *Ora*  
727 *Maritima* indicates that the channels making up such an outlet were then part of a small  
728 tidal delta located at the tombolo, which centuries later would connect the former island  
729 to the mainland, north of Sanlúcar de Barrameda.

730

### 731 6.5. *La Algaida vs Doñana*

732

733 In summary, the genesis and evolution of the two littoral spits flanking the estuary of the  
734 Guadalquivir River rest upon two fundamental, structural conditions other than the fluvio-  
735 marine dynamic constraints of the area: on the one hand, the presence of a Plio-  
736 Pleistocene paleo-relief in the estuary functioning as a sedimentary threshold (Fig. 5); on  
737 the other, the asymmetry of the subsidence processes at work on both sides of the Baetic  
738 front (Fig. 4). As part of the raised tectonic block, south of the LGF, La Algaida was not  
739 affected by these subsidence processes, or at least not to the degree of intensity that these  
740 processes affected the sunken block, north of the fault, where the Doñana spit is located.

741

742 As in other estuaries along the Gulf of Cádiz located in zones of little or no subsidence,  
743 such as the estuaries of the rivers Tinto-Odiel and Guadalete (Dabrio et al., 2000; Goy et  
744 al., 2003), progradation in La Algaida spit during the Holocene has resulted in a system  
745 of successive prograding units that are now exposed above ground. By contrast, the  
746 Doñana spit, north of the LGF, underwent transgressive retrogradation in the first  
747 sedimentary phases of the Holocene due to the sustained, massive subsidence of the  
748 sedimentation. Such was the magnitude of this subsidence that these early deposits remain  
749 below ground at present, covered by subsequent formations which, in a reversed trend,  
750 prograded. The product of this back-and-forth process over the course of the Holocene

751 has been referred to as a retro-aggradational system (Rodríguez-Ramírez et al., 2014). In  
752 effect, the exposed Holocene formations in La Algaida spit are much older than those  
753 above sea level in the Doñana spit, even though the latter is far more extensive. This is a  
754 clear sign of the sedimentary and geomorphological asymmetry registered on either side  
755 of the Baetic mountain ranges. The initial sedimentary phases in the Doñana spit match  
756 progradation phases PS1 and PS2 in the La Algaida spit. As mentioned above, less intense  
757 subsidence processes in the Doñana spit since c. 2000 cal BP facilitated progradation of  
758 this spit over the same time span (Rodríguez- Ramírez et al., 2014). This 2000-year  
759 progradation correlates with Phase PS3 in La Algaida spit.

760

761 It is not easy to find another case in the scientific literature of so clearly a marked  
762 asymmetry between two littoral spits located in the same estuary. The most similar, but  
763 not quite identical, scenarios at hand are located in the Mediterranean basin and on the  
764 coasts of North America. In many littoral areas of the Mediterranean basin, recent  
765 research (Rodríguez-Estrella et al., 2011; Spampinato et al., 2011) has revealed processes  
766 of subsidence and tectonic uplift in the course of the Holocene that have generated  
767 massive depocenters. In the Cascadian subduction zone of the Pacific Plate, investigation  
768 into tectonic activity has enabled researchers such as Nelson et al. (2006) to propose rates  
769 of subsidence and uplift for the Quaternary formations. Along the U. S. Atlantic Coast,  
770 researchers such as Fiaschi and Wdowinski (2020) have concluded that subsidence of  
771 littoral barriers and beaches harbors potentially serious problems for the human  
772 communities settled in those areas, including an increasing rate of sea level rise that may  
773 make the threat of flooding ever more ominous. In the case of subsidence in the area of  
774 the Guadalquivir estuary, however, sea level rise does not seem to pose the same type of

775 threat in the short term, unless present-day climate change dictates otherwise by  
776 compounding the sea-level effect of subsidence.

777

## 778 **7. Conclusions**

779

780 The formation and disposition of a Plio-Pleistocene paleo-relief by the mouth of the  
781 Guadalquivir River have been favored by a system of faults with SW-NE and NNE-SSW  
782 orientation; this paleo-relief is located in the raised tectonic block of the fault system. La  
783 Algaida spit rests on such a paleo-relief.

784

785 In the first half of the fourth millennium BCE (6000 to 5500 cal BP), the sedimentation  
786 of the first Holocene formations took place. These early deposits consisted mostly of  
787 sandy facies that punctuated the evolution of a flood-and-ebb, fluvio/tidal delta under  
788 strong swell influence; this process was conditioned by both the Pliocene paleo-  
789 topography and the intense wave dynamics.

790

791 About the year 3600 cal BP, the evolution of the deltaic system caused the budding barrier  
792 island to finally emerge. In the first millennium BCE, this island would be known by  
793 Phoenician and Greek seafarers, merchants, and colonists as “Cartare island.” It was  
794 separated from the mainland by means of two inlets, which were also outlets of the  
795 Guadalquivir River.

796

797 Shortly after the emersion of the barrier island, a number of units of sedimentary  
798 progradation developed in succession. The first unit (PS1), which grew until around 3000  
799 cal BP, gave the island its earliest form. Thereafter, a second unit (PS2) was initiated and



800 spread, causing the island to expand considerably toward the W and the SW. A third and  
801 final unit (PS3) began to unfold in the first two centuries CE, bringing as a result the  
802 closure of the eastern inlet and the formation of a tombolo that connected the former  
803 barrier island with the mainland.

804

805 The singular morpho-structural traits of the Lower Guadalquivir River Basin have largely  
806 influenced the geomorphological and morpho-stratigraphic characteristics of the  
807 Quaternary formations in the area. The system of faults and alignments has given form to  
808 a somewhat asymmetric estuary in terms of variables such as the sedimentary infilling  
809 and the geomorphological configuration. These variables relate, firstly, to the presence of  
810 a Plio-Pleistocene relief in the estuary which functioned as a sedimentary threshold for  
811 La Algaida spit, and secondly, to the asymmetry of the processes of subsidence at work  
812 on both sides of the Baetic front. As part of the raised block, south of the LGF, La Algaida  
813 avoided most of this subsidence, whereas the Doñana spit, north of the LGF, underwent  
814 subsidence on a large scale. The present result is that while La Algaida exhibits the entire  
815 progradation system of the Holocene as prograding units that are exposed sub-aerially, in  
816 the case of Doñana these formations are buried below sea level. These initial sedimentary  
817 processes in Doñana correlate with progradation phases PS1 and PS2 of La Algaida. By  
818 contrast, in phase PS3, subsidence processes in Doñana were less intense, allowing  
819 progradation to run a course homologous to the progradation then affecting La Algaida.

820

821 Asymmetric sedimentary processes, in combination with the dynamics of neo-tectonics,  
822 make the Guadalquivir estuary and its coastal surroundings a peculiar case for  
823 geomorphological research, and hence a potential reference for future studies elsewhere  
824 on the planet. Although many coastal areas around the world are subject to processes of

825 subsidence and uplift, few, if any, have been considered thus far for hypothetically  
826 comparable conditions of asymmetry impinging upon littoral formations that lie so close  
827 to each other.

828

## 829 **Acknowledgements**

830 We thank the Administration of Espacio Natural de Doñana (END) for the permission to  
831 do fieldwork in areas of special natural protection. The investigation has been made  
832 possible by the financial support of the Regional Government of Andalusia (Junta de  
833 Andalucía) to Research Group RNM276, as well as by funding from the company E2IN2  
834 and entrepreneurs Valentín de Torres Solanot and Manuel Cuevas. The present paper is a  
835 product of Phase III of the Hinojos Project as well as a contribution of Project IGCP 639,  
836 “Sea Level Change from Minutes to Millennia.”. Co-author J. N. Pérez-Asensio thanks  
837 the support of Research Group RNM-190 from Junta de Andalucía. Mr. Joseph P. Pinches  
838 read with attention and improved the final version of the manuscript. We all thank  
839 reviewers and editors of the journal for their helpful comments.

840

## 841 **Figure and table captions**

842

843 Figure 1.- A.- Location of the research area. B.- Tectonic setting (GMF: Guadiamar Fault.  
844 GF: Guadalquivir Fault. LGF: Lower Guadalquivir Fault). C.- Geomorphological outline  
845 with location of cores (A1, A2, A3, A4).

846

847 Figure 2.- Geomorphology of La Algaida spit. Location of cores A1, A2, A3, and A4, and  
848 dates obtained by Rodríguez-Ramírez et al. (1996).

849

850 Figure 3.- Stratigraphy, lithology, dates, benthic foraminiferal abundance (N/g),  
851 planktic/benthic ratio (P/B), and distribution of foraminifera in cores A1 and A2.

852

853 Figure 4.- **A.**- Location of cores and tectonic setting and probable extension of Plio-  
854 Pleistocene paleo-relief. **B.**- Lateral and vertical succession of sedimentary bodies of La  
855 Algaida spit in relation to the Lower Guadalquivir River Fault (LGF), the Plio-Pleistocene  
856 paleo-relief, and the spit of Doñana. (*Y.S.F.*: Yellow sand facies. *G.S.F.*: Gray sand  
857 facies). **C.**- Correlation of analyzed cores in this work with those of Salvany et al., (2011):  
858 (SL, CM, and MA).

859

860 Figure 5.- Evolution of La Algaida from a shoal and swash bars systems to barrier island  
861 and spit. Probable extension of paleo-relief.

862

863 Figure 6.- **A.**- Evolution of the sedimentary transection of the tombolo of La Algaida: a.-  
864 Displacement toward the E of swash bars overlying gray sand facies, b.- Emergence of  
865 tombolo, closure of fluvio-tidal channel, and infilling of estuary, c.- Displacement of the  
866 sedimentary body of the tombolo over the estuary, d.-Progradation of tombolo toward the  
867 ocean, e.- Isolation of tombolo from the marine dynamics. **B.**- Evolution of the  
868 sedimentary transection of the central body of La Algaida: a and b.- Displacement toward  
869 the E of swash bars overlying gray sand facies, c.- Genesis of barrier island (PS1), d.-  
870 Progradation of sedimentary systems PS2 and PS3, e.-Collapse of the spit by a receding  
871 sea and infilling of estuary.

872

873 Table 1: Database of <sup>14</sup>C results after using the Marine 20 curve (Heaton et al., 2020) and  
874 the program CALIB rev. 8.2 (Stuiver and Reimer, 1993). Eight radiocarbon dates were  
875 obtained from mollusk shells at the Accium BioSciences Accelerator Mass Spectrometry  
876 Laboratory (Seattle, USA). Other published radiocarbon data were also used (Rodríguez-  
877 Ramírez et al., 1996).

878

## 879 **References**

- 880 Armijo, R., Benkhelil, J., Bousquet, J.C., Estévez, A., Guiraud, R., Montenat, Ch., Pavillon, M.J., Philip,  
881 H., Sanz de Galdeano, C., Viguier, C., 1977. Chapitre III, Les résultats de l'analyse structurale en Espagne.  
882 Groupe de recherche néotectonique de l'Arc de Gibraltar. L'histoire tectonique récent (Tortonien à  
883 Quaternaire) de l'Arc de Gibraltar et des bordures de la mer d'Alboran. Bull. Soc. Geol. Fr. 7–19, 575–614.
- 884 Barbadillo-Delgado P., 1951. Alrededor de Tartessos: los descubrimientos de La Algaida. Ayuntamiento  
885 de Sanlúcar de Barrameda, Sanlúcar de Barrameda (171 pp.).
- 886 Blanco-Freijeiro, A., Corzo-Sánchez, R., 1983. Monte Algaida. Un santuario púnico en la desembocadura  
887 del Guadalquivir. Historia 16 VIII 87, 123–128.
- 888 Blázquez, A.M., Usera, J., 2010. Palaeoenvironments and Quaternary foraminifera in the Elx coastal lagoon  
889 (Alicante, Spain). Quat. Int. 221, 68–90.
- 890 Boski, T., Camacho, S., Moura, D., Fletcher, W., Wilamowski, A., Veiga-Pires, C., Correia, V., Loureiro,  
891 C., Santana, P. 2008. Chronology of the sedimentary processes during the postglacial sea level rise in two  
892 estuaries of the Algarve coast, southern Portugal. Estuarine, Coastal and Shelf Science 77 (2), 230–244.
- 893 Camacho, S., Boski, T., Moura, D., Scott, D., Connor, S., Pereira, L., 2016. Palaeoenvironmental evolution  
894 of the Guadiana Estuary, Portugal, during the Holocene: A modern foraminifera analog approach. The  
895 Holocene 27 (2): 197-235.
- 896 Confederación Hidrográfica del Guadalquivir (CHG) of Spanish Ministry of Agricultura, Pesca y  
897 Alimentación, 2016. Report...

898 Dabrio, C.J., Zazo, C., Goy, J.L., Sierro, F.J., Borja, F., Lario, J., González, J.A., Flores, J.A., 2000.  
899 Depositional history of estuarine infill during the Late Pleistocene-Holocene postglacial transgression. *Mar.*  
900 *Geol.* 162, 381–404.

901 Dalrymple, R.W., Zaitlin, B.A., Boyd, R., 1992. Estuarine facies models: Conceptual basis and stratigraphic  
902 implications. *J Sedim Petrol* 62:1130–1146.

903 Debenay, J.-P., 1995. Can the confinement index (calculated on the basis of foraminiferal populations) be  
904 used in the study of coastal evolution during the Quaternary? *Quat. Int.* 29–30, 89–93.

905 Dokka, R.K., 2011. The role of deep processes in late 20th century subsidence of New Orleans and coastal  
906 areas of southern Louisiana and Mississippi. *J. Geophys. Res.* 116, B06403, doi:10.1029/2010JB008008.

907 Domínguez Monedero, A.J., 1996. *Los griegos en la Península Ibérica*. Arco, Madrid (96 pp.).

908 Domínguez Monedero, A. J., 2013. Los primeros griegos en la Península Ibérica (s. IX, VI a. C.): mitos,  
909 probabilidades, certezas. In: M. P. de Hoz and G. Mora (Eds.), *El oriente griego en la Península Ibérica:*  
910 *epigrafía e historia*. Real Academia de la Historia, Madrid, pp. 11-42.

911 Esteve-Guerrero, M., 1952. Sanlúcar de Barrameda (Cádiz): factoría de salazón romana en La Algaida.  
912 *Noticiario Arqueológico Hispánico* 1 (1-3), 126–133.

913 Fiaschi, S., Wdowinski, S., 2020. Local land subsidence in Miami Beach (FL) and Norfolk (VA) and its  
914 contribution to flooding hazard in coastal communities along the U.S. Atlantic coast, *Ocean & Coastal*  
915 *Management*, 187, 105078.

916 Flores-Hurtado, E., 1993. *Tectónica reciente en el margen ibérico suroccidental*. (Tesis  
917 Doctoral), Universidad de Huelva (458 pp.).

918 García y Bellido, A., 1993. *España y los españoles, hace dos mil años; según la Geografía de Strábon*, rev.  
919 M. P. García-Bellido. Espasa-Calpe, Madrid (334 pp.).

920 Gavala y Laborde, J., 1959. *La Geología de la Costa y Bahía de Cádiz y el poema “Ora Maritima” de*  
921 *Avieno*. Instituto Geológico y Minero de España, Madrid (315 pp.).

922 Gofas, S., Luque, A.A., Templado, J., Salas, C., 2017. A national checklist of marine Mollusca in Spanish  
923 waters. *Sci. Mar.*, 81(2), 242-254, 10.3989/scimar.04543.21a

924 González-Castillo, L., Galindo-Zaldívar, J., de Lacy, M.C., Borque, M.J., Martínez-Moreno, F.J., García-  
925 Armenteros, Gil, A.J., 2015. Active rollback in the Gibraltar Arc: Evidences from CGPS data in the western  
926 Betic Cordillera. *Tectonophysics* 663, 310-321.

927 Goy, J.L., Zazo, C., Dabrio, C.J., 2003. A beach-ridge progradation complex reflecting periodical sea-level  
928 and climate variability during the Holocene (Gulf of Almeria, Western Mediterranean). *Geomorphology*  
929 50, 251–268.

930 Gutscher, M.A., Malod, J., Rehault, J.P., Contrucci, I., Klingelhoefer, F., Mendes-Victor, L., Spakman, W.,  
931 2002. Evidence for active subduction beneath Gibraltar. *Geology* 30(12), 1071–1074.

932 Heaton, T.J., Köhler, P., Butzin, M., Bard E., Reimer, R.W., Austin W.E.N., Bronk Ramsey, C., Grootes,  
933 P.M., Hughen, K.A., Kromer, B., Reimer, P.J., Adkins, J., Burke, A., Cook, M.S., Olsen, J., Skinner,  
934 L.C., 2020. Marine20—the marine radiocarbon age calibration curve (0-55,000 cal BP). *Radiocarbon* 62. doi:  
935 10.1017/RDC.2020.68.

936 IGME. 1988. Mapa Geológico de España 1: 50·000, hoja 1047, Sanlúcar de Barrameda, Servicio de  
937 Publicaciones del Ministerio de Industria, Madrid.

938 Iribarren, L., Vergés, J., Camurri, F., Fulla, J., Fernández, M., 2007. The structure of the Atlantic–  
939 Mediterranean transition zone from the Alboran Sea to the Horseshoe Abyssal Plain (Iberia–Africa plate  
940 boundary). *Marine Geology*. 243, 97–119.

941 Jackson, N.L., 2013. Estuaries. *Treatise Geomorphol.* 10, 308–327.

942 Kucera, M., 2007. Planktonic foraminifera as tracers of past oceanic environments. In: Hillaire-Marcel, C.,  
943 De Vernal, A. (Eds.), *Developments in Marine Geology*, Vol. 1. Elsevier, Amsterdam, pp. 213–262.

944 Lario, J., Zazo, C., Plater, A.J., Goy, J.L., Dabrio, C.J., Borja, F., Sierro, F.J., Luque, L., 2001. Particle size  
945 and magnetic properties of Holocene estuarine deposits from the Doñana National Park (SW Iberia):  
946 Evidence of gradual and abrupt coastal sedimentation. *Z. Geomorphol.* 45, 33–54.

947 Lario, J., Zazo, C., Goy, J.L., Dabrio, C.J., Borja, F., Silva, P.G., Sierro, F., González, A., Soler, V., Yll,  
948 E., 2002. Changes in sedimentation trends in SW Iberia Holocene estuaries (Spain). *Quat. Int.* 93–94, 171–  
949 176.

- 950 López-Amador, J.J., Ruiz-Gil, J.A., 2010. Las ofrendas del santuario púnico gaditano de La Algaida  
951 (Sanlúcar de Barrameda). In: Mata-Almonte, E. (Ed.), Cuaternario y arqueología: homenaje a Francisco  
952 Giles Pacheco. Diputación Provincial de Cádiz, Cádiz, pp. 271-281.
- 953 Lourens, L.J., Hilgen, F.J., Shackleton, N.J., Laskar, J., Wilson, D.S., 2004. The Neogene Period. In:  
954 Gradstein, F.M., Ogg, J.G., Smith, A.G. (Eds.), A Geologic Time Scale 2004. Cambridge University Press,  
955 Cambridge, pp. 409–440.
- 956 Maldonado, A., Somoza, L., Pallarés, L., 1999. The Baetic orogen and the Iberian-African  
957 boundary in the Gulf of Cadiz: Geological evolution (central North Atlantic). *Mar. Geol.* 155, 9–43.
- 958 Mastronuzzi, G., Sansó, P., 2012. The role of strong earthquakes and tsunami in the Late Holocene  
959 evolution of the Fortore River coastal plain (Apulia, Italy): A synthesis. *Geomorphology* 138 (1), 89–99.
- 960 Medialdea, T., Somoza, L., Pinheiro, L.M., Fernández-Puga, M.C., Vázquez, J.T., León, R., Ivanov, M.K.,  
961 Magalhaes, V., Díaz-del-Río, V., Vegas, R., 2009. Tectonics and mud volcano development in the Gulf of  
962 Cádiz. *Mar. Geol.* 261, 48–63.
- 963 Menanteau, L., 1979. Les Marismas du Guadalquivir: Exemple de transformation d'un paysage alluvial au  
964 cours du Quaternaire récent. (Thèse 3e cycle), Université de Paris-Sorbonne (252 pp.).
- 965 Mela, P. [c. 10-45 EC], 1987. Hispania Antigua en el tratado *De chorographia*. In: Bejarano, V. (Ed.),  
966 Hispania Antigua según Pomponio Mela, Plinio el Viejo y Claudio Ptolomeo; *Fontes Hispaniae Antiquae*  
967 7. Bosch, Barcelona, pp. 1-12, 101-112.
- 968 Mendes, I., González, R., Dias, J.M.A., Lobo, F., Martins, V., 2004. Factors influencing recent benthic  
969 foraminifera distribution on the Guadiana shelf (Southwestern Iberia). *Marine Micropaleontology* 51, 171–  
970 192.
- 971 Morales, J.A., Borrego, J., Jiménez, I., Monterde, J.R., Gil, N. 2001. Morphostratigraphy of an ebb-tidal  
972 delta system associated with a large spit in the Piedras Estuary mouth (Huelva Coast, South-western Spain).  
973 *Marine Geology*, 172: 225-241.
- 974 Morales, J.A., Cantano, M., Rodríguez-Ramírez, A., Martín Banda, R., 2006. Mapping Geomorphology  
975 and Active Processes on the Coast of Huelva (SW Spain). *J. Coast. Res.* 48: 89-99.
- 976 Morales, J.A., 2022. *Coastal Geology*. Springer Nature Switzerland AG, Cham (Switzerland) (463 pp.).

977 Muhs, D.R., Rockwell, T.K., Kennedy, G.L., 1992. Late quaternary uplift rates of marine terraces on the  
978 Pacific coast of North America, southern Oregon to Baja California sur. *Quat. Int.* 15–16, 121–133.

979 Murray, J.W., 1991. *Ecology and Palaeoecology of Benthic Foraminifera*. Longman Scientific & Technical,  
980 New York.

981 Murray, J.W., 2006. *Ecology and Applications of Benthic Foraminifera*. Cambridge University Press,  
982 Cambridge.

983 Nelson, A.R., Kelsey, H.M., Witter, R.C., 2006. Great earthquakes of variable magnitude at the Cascadia  
984 subduction zone. *Quat. Res.* 65 (3), 354–365

985 Ota, Y., Yamaguchi, M., 2004. Holocene coastal uplift in the western Pacific Rim in the context of late  
986 Quaternary uplift. *Quat. Int.* 120 (1), 105–117.

987 Peretti, A., 1979. Il periplo di Scilace. *Studio sul primo portolano del Mediterraneo*. Giardini, Pisa (558  
988 pp.).

989 Pérez-Asensio, J.N., 2021. Quantitative palaeobathymetric reconstructions based on foraminiferal proxies:  
990 A case study from the Neogene of south-west Spain. *Palaeontology* 64, 475–488.  
991 <https://doi.org/10.1111/pala.12538>

992 Pérez-Asensio, J.N., Aguirre, J., 2010. Benthic foraminiferal assemblages in temperate coral-bearing  
993 deposits from the late Pliocene. *J. Foramin. Res.* 40, 61–78.

994 Pérez-Asensio, J.N., Rodríguez-Ramírez, A., 2020. Benthic Foraminiferal Salinity index in marginal-  
995 marine environments: A case study from the Holocene Guadalquivir estuary, SW Spain. *Palaeogeogr.*  
996 *Palaeoclimatol. Palaeoecol.* 560, 110021, doi: <https://doi.org/10.1016/j.palaeo.2020.110021>

997 Pérez-Asensio, J.N., Aguirre, J., Schmiedl, G., Civis, J., 2012. Messinian paleoenvironmental evolution in  
998 the lower Guadalquivir Basin (SW Spain) based on benthic foraminifera. *Palaeogeogr. Palaeoclimatol.*  
999 *Palaeoecol.* 326, 135–151. <https://doi.org/10.1016/j.palaeo.2012.02.014>

1000 Pérez-Asensio, J.N., Aguirre, J., Rodríguez-Tovar, F.J., 2017. The effect of bioturbation by polychaetes  
1001 (*Opheliidae*) on benthic foraminiferal assemblages and test preservation. *Palaeontology* 60, 807–827.  
1002 <https://doi.org/10.1111/pala.12317>.



1003 Pérez-Asensio, J.N., Larrasoña, J.C., Samankassou, E., Sierro, F.J., García-Castellanos, D., Jiménez-  
1004 Moreno, G., Salazar, A., Salvany, J.M., Ledesma, S., Mata, M.P., Civis, J., Mediavilla, C., 2018.  
1005 Magnetobiochronology of lower Pliocene marine sediments from the lower Guadalquivir Basin: Insights  
1006 into the tectonic evolution of the Strait of Gibraltar area. *Geol. Soc. Am. Bull.* 130, 1791–1808.  
1007 <https://doi.org/10.1130/B31892.1>

1008 Pozo, M., Ruiz, F., Carretero, M.I., Rodríguez-Vidal, J., Cáceres, L.M., Abad, M., González-Regalado,  
1009 M.L., 2010. Mineralogical assemblages, geochemistry and fossil associations of Pleistocene-Holocene  
1010 complex siliciclastic deposits from the Southwestern Doñana National Park (SW Spain): A  
1011 palaeoenvironmental approach. *Sediment. Geol.* 225, 1–18.

1012 Rodríguez-Estrella, T., Navarro, F., Ros, M., Carrión, J., Atenza, J., 2011. Holocene morphogenesis along  
1013 a tectonically unstable coastline in the Western Mediterranean (SE Spain), *Quaternary International*, 243,  
1014 (1), 231-248.

1015 Rodríguez-Ramírez, A., Rodríguez-Vidal, J., Cáceres, L.M., Clemente, L., Belluomini, G., Manfra, L.,  
1016 Improta, S., de Andrés, J.R., 1996. Recent coastal evolution of the Doñana National Park (SW Spain). *Quat.*  
1017 *Sci. Rev.* 15, 803–809.

1018 Rodríguez-Ramírez, A., Ruiz, F., Cáceres, L.M., Rodríguez-Vidal, J., Pino, R., Muñoz, J.M., 2003.  
1019 Analysis of the recent storm record in the south-western Spain coast: implications for littoral management.  
1020 *Sci. Total Environ.* 303, 189–201.

1021 Rodríguez-Ramírez, A., Yáñez, C.M., 2008. Formation of chenier plain of the Doñana marshland (SW  
1022 Spain): Observations and geomorphic model. *Mar. Geol.* 254, 187–196.

1023 Rodríguez-Ramírez, A., Flores-Hurtado, E., Contreras, C., Villarías-Robles, J.J.R., Jiménez-Moreno, G.,  
1024 Pérez-Asensio, J.N., López-Sáez, J. A., Celestino-Pérez, S., Cerrillo-Cuenca, E., León, Á., 2014. The role  
1025 of neo-tectonics in the sedimentary infilling and geomorphological evolution of the Guadalquivir Estuary  
1026 (Gulf of Cadiz, SW Spain) during the Holocene. *Geomorphology* 219, 126–140.

1027 Rodríguez-Ramírez, A., Pérez-Asensio, J.N., Santos, A., Jiménez-Moreno, G., Villarías-Robles, J.J.R.,  
1028 Mayoral, E., Celestino-Pérez, S., Cerrillo-Cuenca, E., López-Sáez, J.A., León, Á., Contreras, C., 2015.  
1029 Atlantic extreme wave events during the last four millennia in the Guadalquivir estuary, SW Spain. *Quat.*  
1030 *Res.* 83, 24–40, <https://doi.org/10.1016/j.yqres.2014.08.005>.

- 1031 Rodríguez-Ramírez, A., Villarías-Robles, J.J.R., Pérez-Asensio, J.N., Santos, A., Morales, J.A., Celestino-  
1032 Pérez, S., León, Á., Santos-Arévalo, F.J., 2016. Geomorphological record of extreme wave events during  
1033 Roman times in the Guadalquivir estuary (Gulf of Cadiz, SW Spain): An archaeological and  
1034 paleogeographical approach. *Geomorphology* 261, 103–118,  
1035 <https://doi.org/10.1016/j.geomorph.2016.02.030>.
- 1036 Rodríguez-Ramírez, A., Villarías-Robles, J.J.R., Pérez-Asensio, J.N., Celestino-Pérez, S., 2019. The  
1037 Guadalquivir Estuary: Spits and Marshes. In: Morales J. (Ed.), *The Spanish Coastal Systems*. Springer,  
1038 Cham (Switzerland), pp. 517-541, [https://doi.org/10.1007/978-3-319-93169-2\\_22](https://doi.org/10.1007/978-3-319-93169-2_22).
- 1039 Roy, P. S., Thom B. G., Wright, L. D., 1980. Holocene sequences on an embayed high energy coast: An  
1040 evolutionary model. *Sed Geol* 26:1–19.
- 1041 Royden, L.H., 1993. Evolution of retreating subduction boundaries forms during continental collision.  
1042 *Tectonics* 12 (3), 629–638.
- 1043 Salvany, J.M., 2004. Tilting neotectonics of the Guadiamar drainage basin, SW Spain. *Earth Surface*  
1044 *Processes and Landforms* 29, 145–160.
- 1045 Salvany, J.M., Larrasoña, J.C., Mediavilla, C., Rebollo, A., 2011. Chronology and tectonosedimentary  
1046 evolution of the Upper Pliocene to Quaternary deposits of the lower Guadalquivir foreland basin, SW Spain.  
1047 *Sediment. Geol.* 241, 22–39.
- 1048 Shepard, F.P., 1954. Nomenclature based on sand-silt-clay ratios. *J. Sediment. Petrol.* 24,  
1049 151–158, <https://doi.org/10.1306/D4269774-2B26-11D7-8648000102C1865D>.
- 1050 Soares, A.M., 2015. Datación radiocarbónica de conchas marinas en el golfo de Cádiz: El efecto reservorio  
1051 marino, su variabilidad durante el Holoceno e inferencias paleoambientales. *Cuaternario y Geomorfol.* 29,  
1052 19–29.
- 1053 Spampinato, C.R. Costa, B., Di Stefano, A., Monaco, C., Scicchitano, G., 2011. The contribution of  
1054 tectonics to relative sea-level change during the Holocene in coastal south-eastern Sicily: New data from  
1055 boreholes, *Quaternary International*, 232 (1–2), 214-227.
- 1056 Spanish Ministry of Fomento, 2005. Información climática de nivel del mar. Mareógrafo

- 1057 de Sevilla (Bonanza) (6 pp.).
- 1058 Strabo of Amasya [c. 64 BCE-24 CE], 1966. *Géographie: Tome II (Livres III et IV)*. Laserre, F. (Ed.), Les  
 1059 Belles Lettres, Paris (243 pp.).
- 1060 Stuiver, M., Reimer, P.J., 1993. Radiocarbon calibration program. Rev.4.2. *Radiocarbon* 35, 215–230.
- 1061 Torelli, L., Sartori, R., Zitellini, N., 1997. The giant chaotic body in the Atlantic Ocean off Gibraltar: New  
 1062 results from a deep seismic reflection survey. *Mar. Pet. Geol.* 14, 125–138.
- 1063 Vanney, J.R., 1970. *L'hydrologie du Bas Guadalquivir*. CSIC, Departamento de Geografía Aplicada,  
 1064 Madrid.
- 1065 Viguié, C., 1977. Les grands traits de la tectonique du bassin néogène du Bas Guadalquivir. *Bol. Geol. Min.*  
 1066 88, 39–44.
- 1067 Villalba i Varneda, P., 1986. Introducció. In: P. Villalba i Varneda (Ed.), *Ruf Fest Aviè, Periple [Ora*  
 1068 *Marítima]*. Introducció, text, traducció i notes. Fundació Bernat Metge, Barcelona, pp. 9-67.
- 1069 Villarías-Robles, J.J.R., Rodríguez-Ramírez, A., 2019. The representation of the kingdom of Tartessus by  
 1070 the ancient Greeks revisited: New evidence for a forgotten cause. In: Dellis, J.G., Paipetis, S.A. (Eds.), *The*  
 1071 *Influence of Hellenic philosophy on the contemporary world*. Newcastle upon Tyne (UK), Cambridge  
 1072 Scholars, pp. 204-216.
- 1073 Vött, A., 2007. Relative sea level changes and regional tectonic evolution of seven coastal areas in NW  
 1074 Greece since the mid-Holocene. *Quat. Sci. Rev.* 26, 894–919.
- 1075 Yeager, K.M., Brunner, C.A., Kulp, M.A., Fischer, D., Feagin, R.A., Schindler, K.J., Prouhet, J., Bera, G.,  
 1076 2012. Significance of active growth faulting on marsh accretion processes in the lower Pearl River,  
 1077 Louisiana. *Geomorphology* 153–154, 127–143.
- 1078 Zazo, C., Goy, J.L., Somoza, L., Dabrio, C.J., Belluomini, G., Improta, S., Lario, J., Bardají, T., Silva, P.G.,  
 1079 1994. Holocene sequence of sea-level fluctuations in relation to climatic trends in the Atlantic–  
 1080 Mediterranean linkage coast. *J. Coast. Res.* 10, 933–945.
- 1081 Zazo, C., Dabrio, C.J., Goy, J.L., Lario, J., Cabero, A., Silva, P.G., Bardají, T., Mercier, N., Borja, F.,  
 1082 Roquero, E., 2008. The coastal archives of the last 15 Ka in the Atlantic-Mediterranean Spanish linkage  
 1083 area: sea level and climate changes. *Quat. Int.* 181 (1), 72–87.

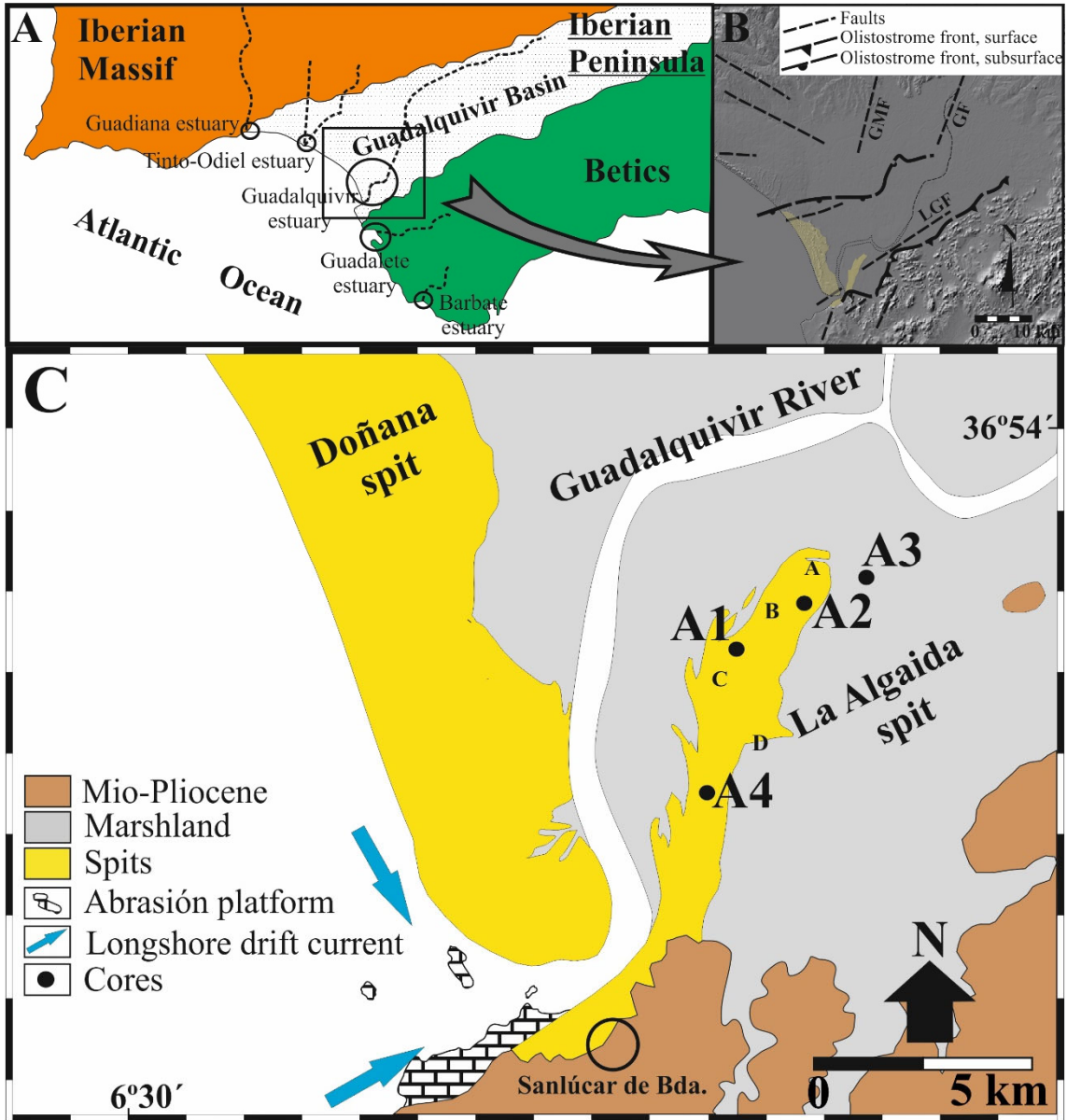
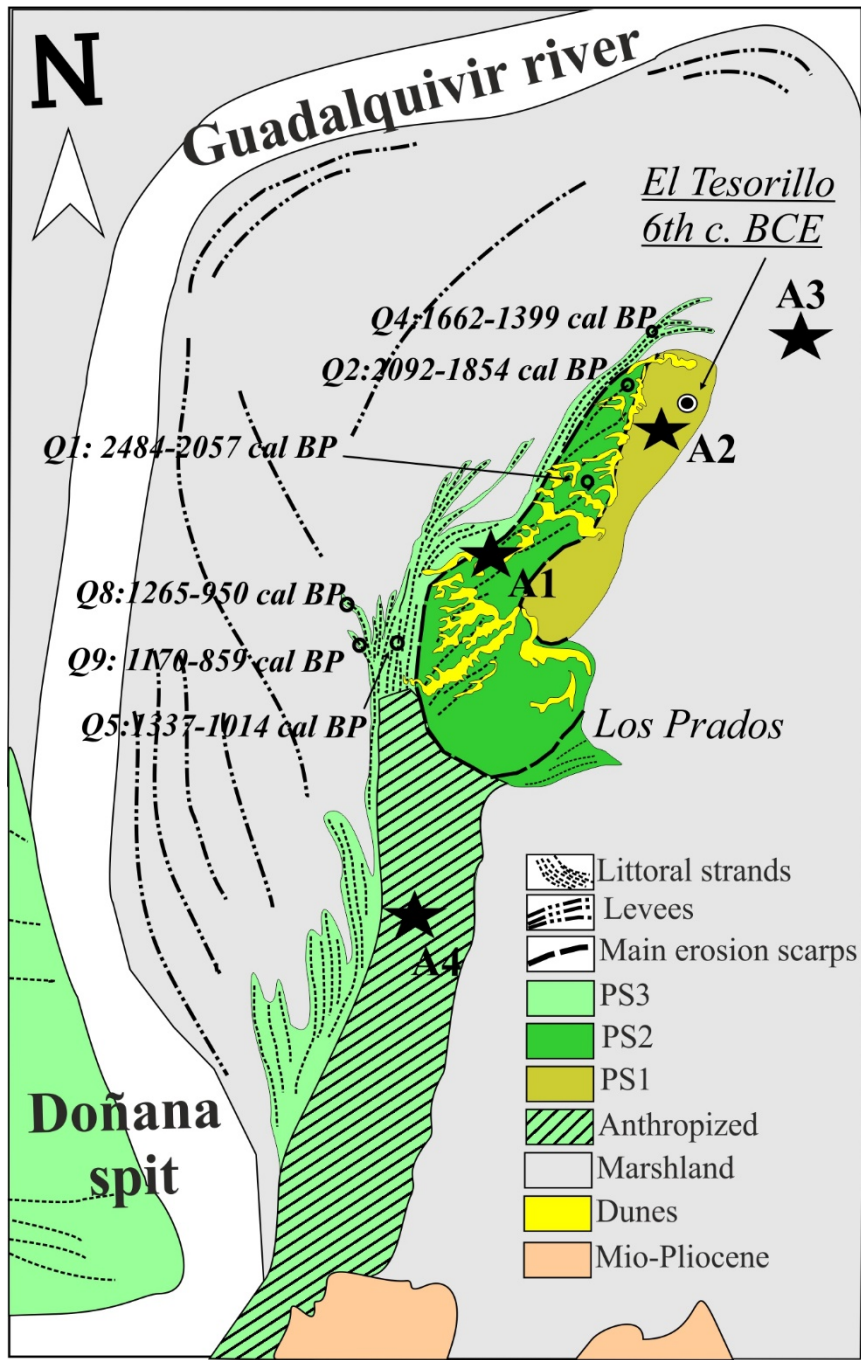


Figure 1.-



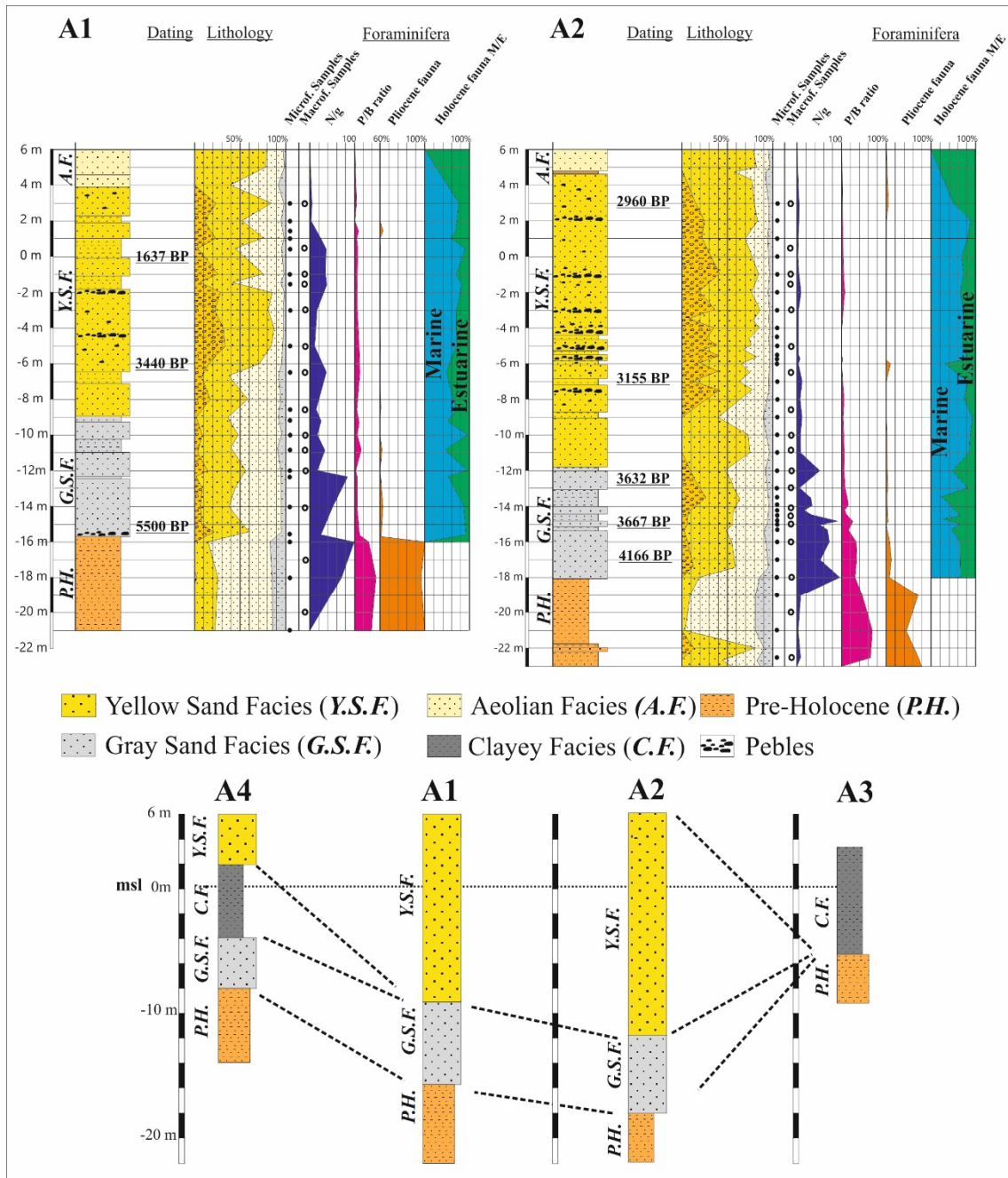
1089

1090

1091

1092

Figure 2.-



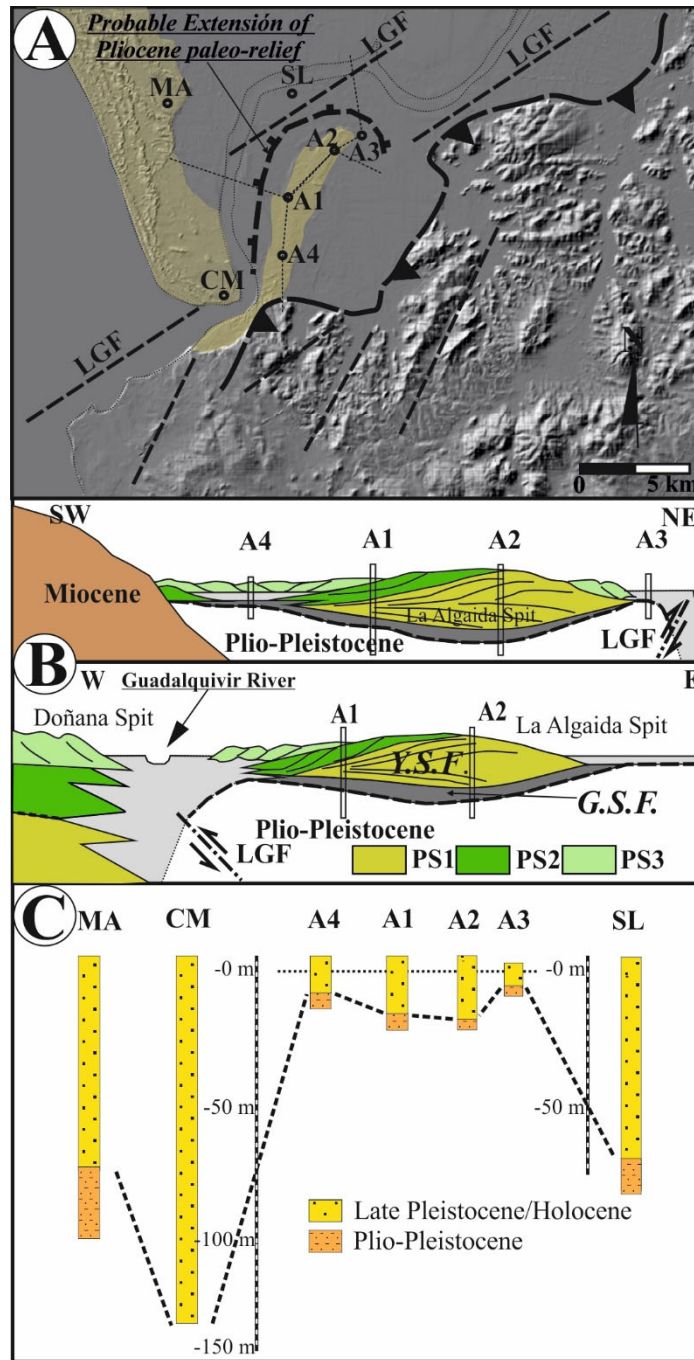
1093

1094

1095

1096

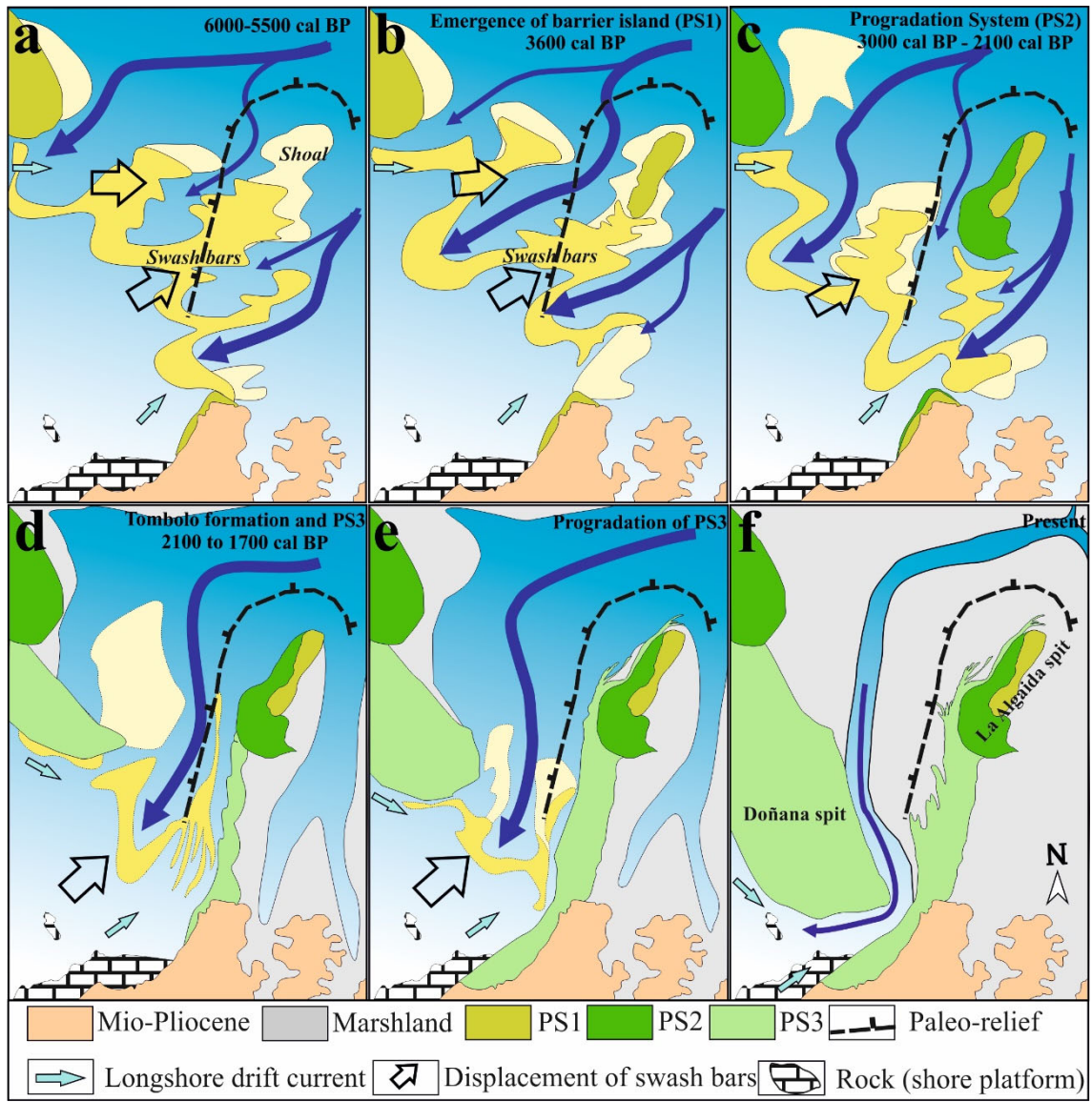
Figure 3.-



1097

1098

Figure 4.-



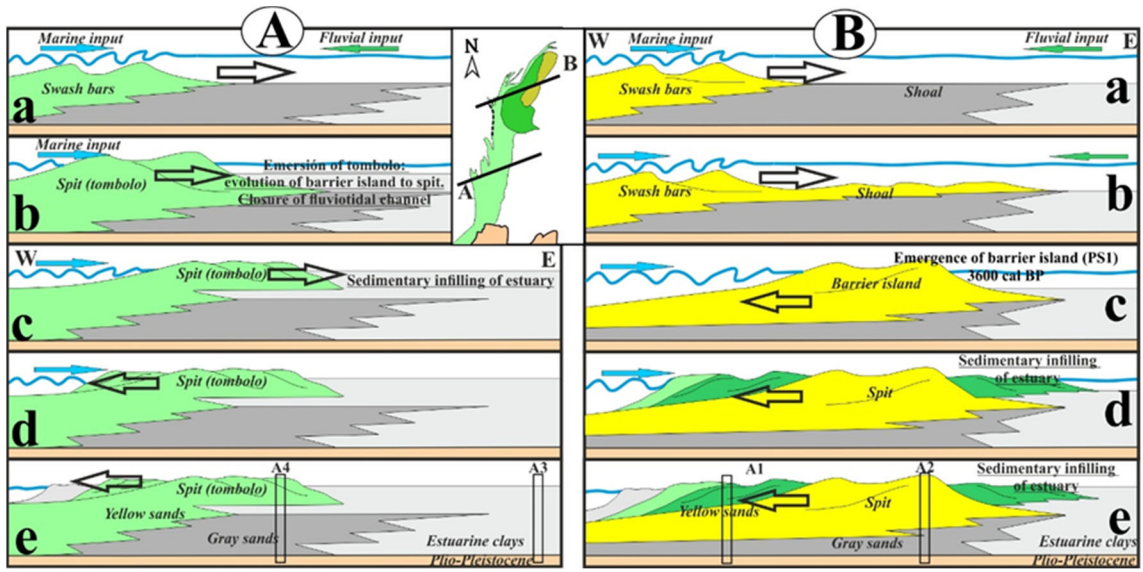
1099

1100

1101

Figure 5.-





1102

1103

1104

Figure 6.-

1105

1106

1107

1108

1109

<b>Location</b>	<b>Depth</b>	<b>Lab. Ref.</b>	<b><sup>14</sup>C yr BP</b>	<b>pMC</b>	<b><sup>14</sup>C cal yr BP (2σ intervals)</b>
A1	-6 m		1955±52	78.40±0.5	<b>1804 - 1501</b>
A1	-12 m	D-AMS 033548	3647±54	63.51±0.42	<b>3723 - 3146</b>
A1	-21.5 m	D-AMS 033549	5032±64	53.45±0.42	<b>5628 - 5316</b>
A2	-3 m	D-AMS 033668	3255±58	66.68±0.48	<b>3249 - 2706</b>
A2	-13.5 m	D-AMS 033669	3417±52	65.35±0.42	<b>3424 - 2860</b>
A2	-18.5 m	D-AMS 033670	3806±54	62.26±0.42	<b>3918 - 3357</b>
A2	-21 m	D-AMS 033671	3834±64	62.05±0.50	<b>3966 - 3373</b>
A2	-23 m	D-AMS 033672	4211±56	59.20±0.42	<b>4454 - 3849</b>
Q1(a)	-0.6 m	B-88022	2487±70	--	<b>2484 - 2057</b>
Q2(a)	-0.5 m	R-2284	2233±29	--	<b>2092 - 1854</b>
Q4(a)	-0.4 m	R-2262	1865±35	--	<b>1662 - 1399</b>
Q5(a)	-0.3 m	B-88021	1530±70	--	<b>1337 - 1014</b>
Q8(a)	-0.4 m	R-88020	1450±70	--	<b>1265 - 950</b>
Q9(a)	-0.2 m	B-88019	1340±60	--	<b>1170 - 859</b>

1110

1111

Table 1